

A Reproduced Copy
OF

N86-13287

LIBRARY COPY

APR 15 1986

LANGLEY RESEARCH CENTER
LIBRARY, NASA
LANGLEY STATION
HAMPTON, VIRGINIA

Reproduced for NASA

by the

NASA Scientific and Technical Information Facility



1 Report No. NASA CR 177361	2 Government Accession No.	3 Recipient's Catalog No.
4 Title and Subtitle Effects of Velocity Profile and Inclination on Dual-Jet-Induced Pressures on a Flat Plate in a Crosswind	5 Report Date October 1985	6 Performing Organization Code
	7 Author(s) A. K. Jakubowski, J. A. Schetz, C. L. Moore and R. Joag	8 Performing Organization Report No.
9 Performing Organization Name and Address Department of Aerospace and Ocean Engineering Virginia Polytechnic Institute and State University Blacksburg, Virginia 24061	10 Work Unit No. T-7526	11 Contract or Grant No. NAG 2-256
	12 Sponsoring Agency Name and Address National Aeronautics and Space Administration Washington, D.C. 20546	13 Type of Report and Period Covered Contractor Report
15 Supplementary Notes Point of Contact: Technical Monitor, Kiyoshi Aoyagi, MS 247-1 Ames Research Center, Moffett Field, CA 94035 (415) 694-5047 or FTS 464-5047		
16 Abstract An experimental study was conducted to determine surface pressure distributions on a flat plate with dual subsonic, circular jets exhausting from the surface into a crossflow. The jets were arranged in both side-by-side and tandem configurations and were injected at 90° and 60° angles to the plate, with jet-to-crossflow velocity ratio of 2.2 and 4. The major objective of the study was to determine the effect of a nonuniform (vs uniform) jet velocity profile, simulating the exhaust of a turbo-fan engine. Nonuniform jets with a high-velocity outer annulus and a low-velocity core induced stronger negative pressure fields than uniform jets with the same mass flow rate. However, nondimensional lift losses (lift loss/jet thrust lift) due to such nonuniform jets were lower than lift losses due to uniform jets. Changing the injection angle from 90° to 60° resulted in moderate (for tandem jets) to significant (for side-by-side jets) increases in the induced negative pressures, even though the surface area influenced by the jets tended to reduce as the angle decreased. Jets arranged in the side-by-side configuration led to significant jet-induced lift losses exceeding, in some cases, lift losses reported for single jets. Jets arranged in tandem induced considerably lower lift losses than side-by-side jets operated under the same conditions. The pressure fields produced by tandem jets featured rapid relaxation of the negative pressures behind the jets, which was suggestive of rapid jet decay rates.		
17 Key Words (Suggested by Author(s)) Dual jet in a crossflow Pressure distribution Jet induced effects	18 Distribution Statement Unclassified - Unlimited STAR Category 02	
19 Security Classif (of this report) Unclassified	20 Security Classif (of this page) Unclassified	21 No of Pages 46
		22 Price*

NASA CONTRACTOR REPORT 177361



Effects of Velocity Profile and Inclination on
Dual-Jet-Induced Pressures on a Flat Plate in
a Crosswind

(NASA-CR-177361) EFFECTS OF VELOCITY
PROFILE AND INCLINATION ON DUAL-JET-INDUCED
PRESSURES ON A FLAT PLATE IN A CROSSWIND
(Virginia Polytechnic Inst. and State Univ.)
52 p HC A04/MF A01

N86-13287

Unclas
CSCL 01A G3/02 01847

A. K. Jakubowski
J. A. Schetz
C. L. Moore
R. Joag

CONTRACT NAC2-256

October 1985

NASA

N86-13287#

NASA CONTRACTOR REPORT 177361

**Effects of Velocity Profile and Inclination
on Dual-Jet-Induced Pressures on a Flat Plate
in a Crosswind**

**A. K. Jakubowski
J. A. Schetz
C. L. Moore
R. Joag**

**Department of Aerospace and Ocean Engineering
Virginia Polytechnic Institute and State University
Blacksburg, Virginia 24061**

Prepared for
Ames Research Center
under Grant NAG 2-256

October 1985

NASA

National Aeronautics and
Space Administration

Ames Research Center
Moffett Field California 94035

ABSTRACT

An experimental study was conducted to determine surface pressure distributions on a flat plate with dual subsonic, circular jets exhausting from the surface into a crossflow. The jets were arranged in both side-by-side and tandem configurations and were injected at 90° and 60° angles to the plate, with jet-to-crossflow velocity ratio of 2.2 and 4. The major objective of the study was to determine the effect of a nonuniform (vs uniform) jet velocity profile, simulating the exhaust of a turbo-fan engine. Nonuniform jets with a high-velocity outer annulus and a low-velocity core induced stronger negative pressure fields than uniform jets with the same mass flow rate. However, nondimensional lift losses (lift loss/jet thrust lift) due to such nonuniform jets were lower than lift losses due to uniform jets. Changing the injection angle from 90° to 60° resulted in moderate (for tandem jets) to significant (for side-by-side jets) increases in the induced negative pressures, even though the surface area influenced by the jets tended to reduce as the angle decreased. Jets arranged in the side-by-side configuration led to significant jet-induced lift losses exceeding, in some cases, lift losses reported for single jets. Jets arranged in tandem induced considerably lower lift losses than side-by-side jets operated under the same conditions. The pressure fields produced by tandem jets featured rapid relaxation of the negative pressures behind the jets, which was suggestive of rapid jet decay rates.

SYMBOLS

A	nozzle exit area
C_p	pressure coefficient, $(P-P_\infty)/q_\infty$
ΔC_p	C_p jet on - C_p jet off
D	jet exit diameter (nominal)
T_L	jet thrust lift
ΔL	jet-induced lift loss
P	static pressure
q	dynamic pressure
\bar{q}	jet-to-crossflow dynamic pressure ratio
R	jet-to-crossflow velocity ratio
Re_D	Reynolds number based on jet exit diameter, $\rho_\infty U_\infty D / \mu_\infty$
Re_l	Reynolds number based on distance from leading edge of plate to jet center, $\rho_\infty U_\infty l / \mu_\infty$
S	nozzle spacing
U	velocity
X	streamwise coordinate with origin at jet orifice center
Y	transverse coordinate with origin in the plane of symmetry of jet configuration
Z	coordinate perpendicular to plate with origin on plate surface
δ	boundary layer thickness
θ	jet injection angle measured from flat plate
μ	viscosity
ρ	density

Subscripts

- freestream crossflow
- j Jet

INTRODUCTION

Jets exhausting into a crossflowing stream are of considerable interest in several engineering applications including V/STOL aircraft in transition flight, vectored thrust nozzles, turbomachinery, combustors and waste disposal. In the case of the V/STOL aircraft, jets exhausting into a crosswind interact with the adjacent surface of the aircraft inducing pressure fields which are responsible for a loss of lift and a change in pitching moment. Most of the prior relevant experimental work has centered on determining the pressure field around a single jet having uniform exit velocity profile [Refs. 1-5]. This pressure field was found to depend strongly on the jet-to-crossflow velocity ratio, R . Dual- and/or multiple-jet configurations which may be important for advanced V/STOL concepts, introduce additional effects concerned with the jet configuration (tandem or side-by-side) and the mutual jet interaction as a function of jet spacing. Studies of these effects have been reported in Refs. 6-7. Another effect which plays an important role in certain VTOL and vectored thrust nozzle concepts concerns the jet injection angle with respect to the crossflow. The first comprehensive investigation of this effect for the case of dual jets, both tandem and side-by-side, has been reported in Ref. 8.

With very few exceptions, VTOL engine exhausts have been simulated by jets having uniform exit velocity profiles. While such an approach allows one to gain understanding of the jet/crossflow interaction and may be useful for making preliminary estimates of the pressure field developed on the surfaces surrounding jets, it does not account for real jet effects such as nonuniformity of the exit velocity profile, swirling, and turbulence of the jet [Ref. 9]. These effects may have a significant influence on the induced pressure field and the resulting aerodynamic loads. The effect of the exit velocity profile may be of particular interest because actual V/STOL engine exhausts are expected to be strongly nonuniform. Kuhlman et al [Ref. 10] investigated the effect of jet decay rate on jet-induced pressures on a flat plate and used cylindrical plugs in the jet nozzle to vary the exit velocity profile. They found that a nonuniform jet with a high velocity in the outer portion of the jet changes the induced pressure field and leads to a smaller nondimensional lift loss than a uniform jet having the same mass flow rate. Ziegler and Wooler [Ref. 11] used annular profile jets with either high velocity - or dead air-cores; they employed jet velocity ratio, R , based on the square root of the dynamic pressure ratio $\sqrt{q_j/q_\infty}$. Their results displayed some differences when compared with the results of Ref. 10; at higher R values, the surface pressure distributions were not strongly affected by the shape of the exit profile.

In the experiments discussed above, only a single jet was used, and the injection was perpendicular to the crossflow. There is clearly a need to investigate further nonuniform jets and to extend such investigations to dual jets and various injection angles. The primary objective of the present work is to obtain information on the surface pressure fields induced by nonuniform dual jets arranged in either a tandem or side-by-side configuration and exhausting at different angles and different velocity ratios. Since the previous investigation of dual jets [Ref. 8] has shown that the mutual jet interaction diminishes rapidly when the nondimensional jet spacing, S/D , increases from 2 to 6, the jet spacings for these

experiments was chosen to be $S/D=2$. Two jet-to-crossflow velocity ratios, $R=2.2$ and 4 , and two injection angles, $\theta=90^\circ$ and 60° , were selected.

In addition to the main objective of this work concerned with the surface pressure measurements, flowfield measurements were made to obtain an insight into the interaction of the jets with both uniform and nonuniform velocity profiles. These measurements were limited to the dual tandem jets exiting at 90° and involved mapping velocity vectors in the plane of symmetry of the configuration.

APPARATUS

The experiments were performed in the Virginia Tech subsonic closed-circuit Stability Wind Tunnel which has a test section $1.83\text{ m} \times 1.83\text{ m}$ ($6\text{ ft} \times 6\text{ ft}$). The tunnel velocity ranged from 8.6 m/sec to 40.5 m/sec (28.3 ft/sec to 132 ft/sec). The wind tunnel is described in Ref. 12.

The test model consists of a steel flat plate fitted with a $60.96\text{ cm} \times 71.12\text{ cm}$ ($24\text{ in} \times 28\text{ in}$) instrumented section (Fig. 1). The latter has an "L" shaped cutout to accommodate various nozzle and spacer sections to realize various injection angles and a variety of either tandem or side-by-side jet configurations. The flat plate model has an elliptical leading edge and a tapered trailing edge. Since the model was designed for testing in the $2.13\text{ m} \times 3.05\text{ m}$ ($7\text{ ft} \times 10\text{ ft}$) Subsonic Wind Tunnel at the NASA Ames Research Center, it was necessary to modify one side wall of the test section of the Virginia Tech $1.83\text{ m} \times 1.83\text{ m}$ ($6\text{ ft} \times 6\text{ ft}$) wind tunnel to allow a small part of the model to protrude. The flat plate was mounted 40.64 cm (16 in) below the tunnel ceiling with the jets exhausting downward. The jet nozzles had a 4.93 cm (1.94 in) exit diameter. The center of the front jet nozzle was located 48.26 cm (19 in) behind the flat plate leading edge. The boundary layer on the plate was tripped using a 5.08 cm (2 in) wide strip of 100 grit sandpaper.

Each of the two air jets was produced by a set of two axial blowers; a larger blower rated at $40\text{ m}^3/\text{min}$ (1400 CFM) supplied the outer, high-velocity portion of the jet, and a smaller one rated at $8.5\text{ m}^3/\text{min}$ (300 CFM) supplied the inner, low-velocity portion of the jet. Both blowers were driven by DC electric motors; this allowed control of the mass flow rates by simply adjusting the supply voltage. The outputs of the two large and two small blowers, respectively, were matched exactly by rheostat control of the supply voltage. The blowers were connected to the nozzles by means of flexible plastic tubes. The nozzle assembly is shown in Fig. 2 for the case of the 90° injection angle. The main components of the assembly are two concentric tubes through which air is forced by the blowers, an injector chamber within the exit nozzle, and a removable stream separation insert. This insert, attached to the inner tube, can be translated axially to control the separation of the inner, low-velocity stream from the outer, high-velocity stream prior to reaching the nozzle exit and, hence, to control the shape of the exit velocity profile. The jet exit profiles can be varied over a wide range of shapes by controlling the mass flow rates of the blowers and adjusting the position of the stream separation insert. A uniform velocity profile can be readily obtained by removing the separation insert and reducing the mass flow rate through the inner tube.

The main instrumentation in these experiments consisted of static pressure taps whose layouts are shown in Fig. 3(a) and 3(b) for the side-by-side and tandem jet configuration, respectively. These layouts were chosen to minimize the overall number of the pressure taps. In addition, selection of the layout pattern was influenced by an assumption that for both jet configurations, the symmetry of the flowfield and the resultant surface pressure field would be good. The side-by-side configuration used a total of 312 pressure taps, while the tandem configuration employed 318 taps. Individual pressure taps were connected by long plastic tubing to ten Scanivalves fitted with dummy transducers. The pressure output from each of the Scanivalves was fed by a short line to one port of a 12-port wafer switch. The latter was connected directly to a single differential pressure transducer (PDCR-22) having a range of $\pm 6.895 \times 10^3$ Pa (± 1 psi). This measuring system, based on sharing a single pressure transducer, has a slower rate of data acquisition than a regular non-sharing system (with each Scanivalve fitted with an active transducer), however, it offers an advantage of possibly higher accuracy, particularly when measuring small pressure differentials. All the pressures were referenced to the freestream (wind tunnel) static pressure. The step time from one pressure port to the next one was 2 seconds. This step time was established on the basis of extensive preliminary experiments in which the pressures at selected locations were continuously recorded at a high rate. In most cases, fully stabilized pressures were reached after a period of 0.5 to 1 second. To obtain a good mean value, the static pressures at each port were computer averaged during the last second prior to stepping to the next port. The pressure transducer was calibrated after every 46 consecutive pressure measurements. The calibration involved zero- and 1.00 psia - pressure readings. The 1.00 psia pressure was supplied by a precise dead-weight tester. The updated calibration information was fed into the computer which processed the pressure data.

In addition to surface pressure measurements, pressures and temperatures were taken for the air flows of the jets, tunnel freestream flow and the barometric conditions.

To obtain time-averaged velocity measurements in the plane of symmetry of the transversely injected tandem dual jets, a five-port yawhead probe was used. The probe was mounted on a traverse mechanism and was oriented at 45° with respect to the flat plate. The probe was located about 51 cm (20 in) upstream of the attachment on the traverse mechanism and the effect of the probe support on the probe measurements was considered to be minimal.

All the measured data were recorded and processed by an HP 3052A Data Acquisition System.

TEST CONDITIONS AND PROCEDURES

The major parameters in testing dual jet configurations are jet-to-freestream velocity ratio (R), jet injection angle (θ), and the jet spacing (S). Based on previous experiments with the same flat plate model [Ref. 8], a constant dimensionless jet spacing, $S/D=2$, was selected; this was the smallest spacing allowed by the experimental set up. Two jet injection angles, $\theta=50^\circ$ and 60° , were chosen. The range of jet-to-crossflow velocity

ratio was constrained by (a) the maximum output of the blowers and (b) the lowest wind tunnel velocity (about 10 m/sec (30 ft/sec)) to develop turbulent boundary layer near the jet injection. The above two conditions determined the maximum R value of 4. For the lowest velocity ratio R, a value of 2.2 was chosen, for which experimental results obtained with uniform jets are available. The velocity ratio, R, was changed by varying the tunnel speed while holding the jet velocity fixed. This procedure eliminated the difficulties associated with duplicating the nonuniform jet velocity profiles at different jet speeds.

The jet exit velocity profiles used in these experiments are shown in Fig. 4. These profiles were measured in the absence of the crossflow using a traversing Pitot-static probe. The nonuniform velocity profiles were selected to represent the case of a turbo-fan engine. The equivalent uniform-velocity jet had approximately the same mass flow rate as the nonuniform jet. To satisfy this condition, the equivalent velocity of the uniform jet was determined from

$$u_{eq} = (1/A) \int_A u dA$$

where u is the velocity and A is the nozzle exit area. It can be seen from Fig. 4 that the symmetry of the nonuniform profile was better for the inclined injection ($\theta=60^\circ$) than for the transverse ($\theta=90^\circ$) injection. In addition, the average velocity of the 60° jet was somewhat higher than for the 90° jet. This increase in the velocity was made possible due to small modification in the ducting connecting the blowers to the nozzle assemblies. By removing sections originally intended for mass flow measurements, the pressure drop in the duct lines was reduced, and the jet velocity was raised somewhat. This, in turn, allowed raising the tunnel velocity (for the experiments with 60° jets) which might have a favorable effect on the quality of data because of increased values of the measured pressures and/or possible improvement of the boundary layer characteristics. The tunnel and jet velocities used in these experiments are listed in Table 1.

The boundary layer profiles at the front nozzle location were determined by means of a 21-tube rake. The nondimensional profiles shown in Fig. 5 correspond to the tunnel velocities used in the 90° tests. The freestream Reynolds number based on the surface distance to the front nozzle, Re_x , was below a value required to have natural transition and a fully developed turbulent boundary layer, so a sand paper strip trip was used. The profiles in Fig. 5 appear to be typical for artificially tripped boundary layers.

The jet induced pressures on the flat plate were determined as the difference between jet-on and jet-off conditions. The experimental procedure consisted of the following major steps:

- (1) reading surface pressures at a desired crossflow velocity with the jets off and nozzles plugged with inserts flush with plate surface,
- (2) checking the velocity of each jet with the tunnel off by traversing a Pitot-static tube in small increments along the x- and y-direction across the nozzle exit area,
- (3) recording surface pressures with the jets and tunnel turned on; the readings were started after the jet air temperature had stabilized at a

TABLE 1

Freestream and Jet Flow Conditions

Jet inclination angle θ , deg.	Jet-to-crossflow velocity ratio R	Tunnel velocity m/s(ft/s)	Freestream Reynolds number		Jet velocity, m/s (ft/s)		
			Re_D ($\times 10^{-5}$)	Re_λ ($\times 10^{-5}$)	Uniform jet	Nonuniform jet	
						Peak velocity in outer region	Av. velocity in inner core
90	2.2	15.7 (51.5)	0.45	4.4	34.4 (113)	55.2 (181)	18.9 (62)
	4	8.6 (28.3)	0.24	2.5			
60	2.2	18.3 (60)	0.52	5.2	40.2 (132)	58.8 (193)	23.5 (77)
	4	10.1 (33)	0.29	2.9			

- constant temperature which was about 30°F higher than the freestream tunnel temperature,
- (4) after the surface pressures had been taken, the tunnel was turned off and the jet velocities were checked again.

RESULTS AND DISCUSSION

The surface pressures induced by the jets are presented in the nondimensional form as

$$\Delta C_p = C_{p \text{ jet on}} - C_{p \text{ jet off}}$$

where $C_p = (P - P_\infty)/q_\infty$ and freestream values of the static (P_∞) and dynamic (q_∞) pressures are used as reference conditions. Because of the symmetry of the jet/crossflow arrangement, the induced pressure field was expected to be symmetrical. On this basis, the actually measured pressure data were extended to a larger surface area by reflecting the actual data points about the line of symmetry in each configuration to generate virtual data points in the noninstrumented regions of the plate. Both actual and virtual data points were used to generate constant pressure contours of the induced pressure field. From inspection of Fig. 3 it can be seen that, for the side-by-side configuration, the virtual data points were generated in the right-hand portion of the flat plate surface, while for the tandem configuration, the virtual data points were created in the left-hand portion of the graph. Consequently, some caution should be exercised when analyzing pressure fields in those areas.

Generating constant-pressure contour plots can be a tedious and time-consuming task which, in addition, may involve an element of subjective judgement. In an effort to alleviate these problems, we employed a Cal Comp General Purpose Contouring Program to trace out isobar contour maps. While the computer tracing worked quite well inside the regions covered by a large number of input data points, the parts of the plots near the inner and outer boundaries were found to be unsatisfactory. Therefore, the contour maps presented in the following sections were made by hand plotting using computer generated layouts of the numerical pressure data. For details on computer plots see Appendix A.

Jets Exiting at 90°

The surface pressure distributions obtained with side-by-side jets exhausting at $\theta=90^\circ$ into the crossflow are shown in Figs. 6-9.* Generally, the pressure fields induced by the 90° jets display small regions of slightly positive pressures ahead of each jet and very large negative-pressure region to the sides of and downstream of the jet nozzles. Lack of left-to-right symmetry (for each jet) of the pressure contours near the jet exits indicates clearly that the flowfields produced by the jets strongly

*Broken lines represent contour sections determined by extrapolation of the measured data.

influence each other; this results from the fact that transverse jets induce large negative-pressure fields projecting over large distances not only to the sides of the jets but in the upstream direction as well.

The effects of increasing the jet-to-crossflow velocity ratio, R , from 2.2 to 4 can be seen by comparing Fig. 6 with Fig. 7 and Fig. 8 with Fig. 9. For uniform velocity-profile jets (Figs. 6 and 7), the negative-pressure region expands in nearly all directions. Based on the surface area enclosed by the $\Delta C_p = -0.3$ line, this expansion is about 70% of the area corresponding to $R=2.2$. For nonuniform velocity-profile jets, the increase in the negative-pressure area, caused by increasing R , is smaller, estimated crudely at about 30%, and is characterized by a forward shift of the negative pressure center. The small positive-pressure regions ahead of the jets appear to decrease significantly when the parameter R is increased from 2.2 to 4. A similar effect of the parameter R on the induced negative-pressure field has been documented in previous experiments with single and dual jets exiting normally into a crossflow [Refs. 1-8]. An increase in R causes the negative-pressure region to expand and the pressure center to move forward.

A simple physical explanation of the effects of the parameter R may be given by taking a close look at the mixing/interaction process between a single jet and crossflow (Fig. 10). This mixing/interaction is a highly complex, unsteady process involving development of turbulent structures of various scales and lifetimes at the jet/crossflow interfaces. In a time-averaged frame, the mixing/interaction reduces mostly to three major, interrelated aerodynamic effects [Ref. 9]:

- (a) the turbulent entrainment of air from the crossflow leading to, among other things, a rapid spread of the jet. The entrainment of crossflowing air by the jet creates a low-pressure region around the nozzle and this effect becomes more pronounced as the parameter R increases:
- (b) a pair of counter-rotating vortices formed in the jet as it emerges from the nozzle; these vortices tend to control the downstream development of the jet. The effect of counter-rotating vortices influences mostly the surface pressure distribution downstream of the jet center. Since the vortices arise, it is suggested, from the shearing action exerted by the crossflow on the sides of the jet as the latter emerges from the nozzle, the vortex strength is likely to increase with increasing initial upright distance and penetration (and, hence, with increasing R) of the jet before it is bent in the crossflow direction. Therefore, increasing R results in a growing vortex intensity which in turn leads to larger induced velocities and increased surface area influenced by the jet. However, this trend is not expected to continue indefinitely. When R reaches and then exceeds a certain value (for instance, around 8), the effect of a further vortex strength increase will not be felt anymore on the surface because it becomes nullified by the concurrent effect of the vortex centerline being displaced further away from the surface. If the parameter R continues to increase, the initial trend in the effect of the counter-rotating vortices on induced surface pressures is expected to become reversed, resulting in reduced surface area influenced by the jet.

(c) a blockage effect caused by the jet and resulting in a near-surface wake behind the jet. The blockage effect results in a positive-pressure region ahead of the jet, a streamwise acceleration (and, hence, lower pressures) near the sides of the nozzle and a wake flow behind the jet, where a significant entrainment activity takes place. As R increases, the effect of the blockage tends to diminish (except for the range of R less than about 0.5, which is of little importance to VTOL applications), and we may expect that the forward positive-pressure region and the acceleration near the nozzle sides decrease, while the wake region will remain only weakly affected. The overall effect of blockage on the surface pressures, corresponding to an increase of R , may be one of (1) positive-pressure region becoming smaller, (2) pressures near the nozzle sides becoming somewhat less negative, and (3) wake region remaining almost unchanged or somewhat reduced, primarily due to changes in the Reynolds number based on crossflow conditions and the nozzle size.

Summarizing the individual effects of entrainment, the vortex pair and blockage it is concluded that the expected resultant changes in the surface pressure field, when R is increased, are as follows:

(1) the negative-pressure regions to the sides of the nozzle expand until a certain R is reached, beyond which a reverse trend may be expected,

(2) the generally small positive-pressure region ahead of the jet decreases continuously, and

(3) the effective center of the pressure field which at low R values is located downstream of the nozzle, moves continuously forward, approaching the nozzle center at high R values. This trend is suggested by the fact that at high R values, the entrainment effect which, per se, tends to develop a negative-pressure field symmetrical with respect to the nozzle center, becomes very likely the main contributor to the pressures over most of the surface except for the regions ahead of and behind the jet nozzle where the blockage effects dominate. While the discussion just presented refers to a single jet, similar arguments may be applied to a case of dual jets.

Returning now to our results shown in Figs. 6-9, it can be seen that the experimentally observed trends are consistent with the physical explanation given in the preceding discussion. Since no data were obtained for R values higher than 4, the prediction concerning the behavior of the pressure field at high R could not be verified. However, careful examination of the pressure plots in Ref. 8 indicates that while an increase of R from 4 to 6 resulted in a significant increase of the surface area influenced by the jet for both tandem and side-by-side dual jet configurations, a further increase of R from 6 to 8 seemed to produce a slight contraction of the jet-influenced surface area for tandem jets, and only a small or moderate expansion of this area for the side-by-side jets.

The influence of the jet velocity profile on the pressure fields induced by the 90° jets can be seen in Figs. 11 and 12. The nonuniform velocity-profile jets induce larger negative-pressure regions (and smaller upstream positive-pressure regions) and the pressures near the jet nozzles are consistently lower for such jets. At $R=2.2$, the negative-pressure area (enclosed by the $\Delta C_p = -0.3$ line) is about 50% larger for the nonuniform jet, and at $R=4$, this increase is roughly estimated at about 20%. It can be seen

that the trends of these changes are the same as those which result from increasing R. It is suggested that these changes may be explained as follows:

The nonuniform jets used in this study have significantly higher dynamic pressure ratio

$$\bar{q} = \rho_j U_j^2 / \rho_\infty U_\infty^2$$

than the uniform jets; the ratio $\bar{q}_{\text{nonuniform}} / \bar{q}_{\text{uniform}}$ is about 1.7 and 1.5

for the 90° and 60° jets, respectively. The higher \bar{q} of the nonuniform jet results in an increased penetration height and higher trajectory of the nonuniform jet* [Ref. 13]. The higher penetration makes the jet acquire characteristics of a jet originating with a higher effective R: the initial entrainment and the initial vortex pair become stronger (because of higher penetration), while the blockage is reduced. These effects should result in a pressure field upstream of the jet resembling a higher "effective" R case. At the same time, the higher trajectory combined with the faster decay rate of the nonuniform jet lead to reduced jet effects on the pressure field in the region behind the jet and quicker relaxation of the induced pressures behind the nozzles. Such an effect can be seen in Fig. 12; the negative pressures induced by the nonuniform jets relax faster than those induced by uniform jets having the same nominal velocity. The faster decay of the nonuniform jets may be explained by enhanced turbulent mixing occurring in nonuniform jets.

Additionally, it may be argued that the nonuniform jets used in these experiments are viewed by the approaching crossflow as jets having effectively higher velocity than the uniform jets. It is the outer, high-velocity portion of each jet that first comes in contact and interaction with the crossflow, and, as such, it may play a dominant role in establishing the initial (i.e., upstream of and near the jet exits) flowfield and the pressures induced on the surface. It takes some distance that the jet must travel from the nozzle exit before the crossflow enters an effective mixing and interaction with the inner (originally low-velocity) portion of the nonuniform jet. As a consequence of such a development, the initial jet/crossflow mixing/interaction which is responsible for the pressure field upstream of the front jet may exhibit features characteristic of a higher effective R value, such as increased regions of negative pressures and reduced regions of positive pressures. The remaining portion of the pressure field may become influenced by the interaction of the crossflow with the entire jet including its inner core which results in a more rapid jet decay and a faster relaxation of the induced pressures behind the jet nozzles.

*The penetration height also depends on the peripheral-to-core velocity ratio. The latter remained nearly constant throughout these experiments.

Because the nonuniform jets induce: (a) a larger negative-pressure region projecting further in the upstream direction and/or decaying faster behind the jet nozzles, and (b) smaller positive-pressure regions ahead of each jet, the resultant induced pressure force has a more forward location than that for a uniform jet arrangement. This may reduce a nose-up pitching moment on the aircraft.

The pressure field induced by the tandem configuration of 90° jets is presented in Fig. 13 for the case of uniform profiles at $R=2.2$. The data obtained for the other 90° tandem jets cases have been judged to be of less accuracy and are not included. Discussion of pressures induced by tandem 90° jets is presented in Section "Tandem Jets at 60°."

Side-by-Side Jets at 60°

Uniform-Velocity-Profile Jets

Figure 14 shows the surface pressure field induced by the side-by-side inclined jets ($\theta=60^\circ$) having uniform velocity profiles and relatively low jet velocity ($R=2.2$). The interaction between the two jets over a distance from $X/D=-1.5$ to $X/D=3$ seems to be relatively weak. The pressure distributions in front of and behind each jet (with the obvious exception of the region along the longitudinal centerline of the whole configuration) display features resembling those of single jets; i.e. approximately symmetrical left-to-right, positive ΔC_p region (for $\Delta C_p > +.2$) and nearly symmetrical pressure contours near and behind the nozzles with two downward projecting lobes. Between the lobes, in the lee of the jets, the contours are pulled back closer to the jet nozzles indicating low velocity (less negative ΔC_p) flow regions. Further downstream (around $X/D=3$), both jets start to interact strongly which is reflected in a merging of the pressure lobes near the longitudinal centerline of the side-by-side arrangement.

As the parameter R increases from 2.2 to 4, the overall area of the surface influenced by the jets increases strongly (Fig. 15). The negative pressure area enclosed by the $\Delta C_p = .3$ line increases approximately 150%, relatively large (at $R=2.2$) positive pressure regions ahead of the jets, enclosed by the $\Delta C_p = +.1$ line reduce about 50% and the pressure center moves slightly more downstream from the nozzle exit.

As the jet influence increases (when R changes from 2.2 to 4), so does the interaction between the jets. As a result, the left-to-right symmetry of the pressure contours near the jet nozzles deteriorates and, except for the very strongly negative pressure region ($\Delta C_p = -2.0$), most of the pressure lines of the two jets merge and, in a sense, the configuration starts behaving as a single jet of combined capacity. In the region between the jets, along the centerline of the configuration, the effects of both jets superimpose, this results in very low pressures, i.e., high velocities near the surface between the jet nozzles and near downstream.

When compared with the 90° jets, the 60° angled jets display the following changes:

- (a) The surface area influenced by the jets is reduced. At $R=2.2$, the surface area enclosed by the line of $\Delta C_p = -0.3$ is about 40% smaller; at $R=4$, the corresponding area is roughly 10% smaller for the 60° jets,
- (b) The pressures near the jet nozzles are significantly reduced and become strongly negative. From Figs. 6, 7, 14 and 15, it can be seen that in the lateral direction, the pressures near the 60° jet nozzles are lower than those near the 90° jet nozzles within a radius of 1.5 D and 2.5 D for the cases of $R=2.2$ and 4, respectively,
- (c) The left-to-right symmetry of the pressure contours near the jet exits improves significantly.

The above changes may be explained by the following effects brought about by inclination of the jets (Fig. 16):

- (a) The presence of a horizontal (parallel to the surface) component of the jet velocity which imparts a strong acceleration to the crossflow near the jet boundaries leading to very low pressures.
- (b) A reduction of the vortex pair strength and hence the induced flowfield velocities. The vortex strength reduces with decreasing jet inclination angle, θ , because it is the crossflow velocity component normal to the jet which is mostly responsible for the vortex creation. The reduced vortex strength results in a reduced lateral expansion of the surface area influenced by the jet even though the smaller penetration of the inclined jet* tends to oppose or moderate this trend.
- (c) A reduction of the "solid-wall" blockage due to inclination and smaller penetration of the jet, and a possible reduction in air mass entrainment rate due to the reduced vortex pair strength. These effects tend to contribute to a further decrease in the surface areas influenced by the jet.

While the combined result of these effects is expected to indicate a reduced surface area affected by the 60° jets (versus 90° jets), the effect of the jet inclination θ on the magnitude of the resultant pressure force may be difficult to predict, as it may represent a delicate balance of two opposing trends. The surface area affected by the jet decreases with decreasing θ while the absolute value of the negative pressures near the nozzle increases strongly. The net result is expected to depend on factors such as the jet exit velocity distribution and swirl and turbulence characteristics of the jet. These factors are likely to control the behavior and decay rate of the jet and thus the jet/crossflow interaction.

In our experiments with dual jets, acceleration of the crossflow near the nozzles (i.e., effect (a)) appears to predominate, and the net negative pressure force is larger (leading to a larger loss in the lift force), for the 60° jets, particularly at the higher R value ($=4$), even though the overall surface area influenced by the negative pressures is greater for the 90° jets.

*The jet penetration is controlled by the vertical component of the jet exit velocity.

The improved left-to-right symmetry of the pressure contours near the jet exits, as the angle θ is changed from 90° to 60° , is a direct consequence of the reduced outward range of influence of the 60° jets; their negative-pressure region is smaller in general and projects less in the upstream direction, making the mutual jet/jet interference weaker for the 60° jets.

Nonuniform Velocity-Profile Jets

The pressure plots obtained with jets having nonuniform exit velocity profiles are shown in Figs. 17 and 18 for the cases of $R=2.2$ and 4, respectively. Comparison of the pressure contours in Figs. 17 and 18 with those in Figs. 14 and 15 indicates that the patterns obtained with nonuniform and uniform jets are generally similar for the same R . However, the negative-pressure region to the side of and behind the jets (and consequently the expected lift loss) is increased for the nonuniform jets. The positive-pressure regions ahead of the jets are reduced for the nonuniform jets. For $R=2.2$, the region of nonuniform-jet induced negative pressures, based on the $\Delta C_p = -.3$ line, is estimated to be about 50% larger than that for the uniform jets. The concurrent reduction of the positive-pressure regions, based on the $\Delta C_p = +.1$ line, is roughly estimated at about 30%. For $R=4$, the corresponding estimates are about 35% increase in the negative-pressure region and about 75% reduction in the positive-pressure regions. These changes may be explained by similar physical arguments as those presented in the section discussing 90° jets.

The pressure contours in Fig. 17 indicate two regions of slightly positive pressures downstream of the large negative-pressure region. These regions may be indicative of near-surface recirculating or reverse-flow zones behind the jet exhausts. It is interesting that a similar, though much weaker, feature may be present in the corresponding case ($R=2.2$) of the uniform jets (see the $\Delta C_p = 0$ lines in Fig. 14).

The effects of increasing R in the nonuniform jet configuration can be seen by comparing Figs. 17 and 18. These effects are quite similar to those observed with uniform jets. When R is increased from 2.2 to 4, the negative pressure area increases about 130%, somewhat less than for the uniform jets. The forward positive-pressure areas decrease about 90%. As R increases, the jet velocity component parallel to the surface increases correspondingly leading to very high negative ΔC_p values, such as -7.0 near the jet exits (Fig. 18).

Figure 19 shows the jet-induced lift loss for the side-by-side configurations. The lift loss has been calculated by integration of the pressure data obtained for a square area extending from $Y/D = -2$ to 4 and from $X/D = -2$ to 4. This area is equal to 24.4 times the jet exit flow area. The pressures in the noninstrumented corners of this area have been assumed from extrapolations. Because the contribution of these pressures to the overall net pressure force is, in most cases, relatively small, errors involved in these extrapolations should not cause any significant errors in the lift loss evaluation. The lift loss, ΔL , has been nondimensionalized by the

calculated lift due to jet thrust, T_L . The latter was calculated for nonuniform jet from

$$T_L = \sin \theta (\dot{m}_0 U_0 + \dot{m}_1 U_1)$$

where \dot{m}_0 - mass flow rate of outer flow
 \dot{m}_1 - mass flow rate of inner flow
 U_0 - averaged velocity of outer flow
 U_1 - averaged velocity of inner flow

The lift loss data in Fig. 19 indicate a few important effects. First, closely spaced dual jets result in significant lift losses, comparable to or greater than those typically reported for the single jets. Second, the 60° angled jets induce considerably larger lift loss than the 90° jets. Only a part of this increase may be attributed to the reduction of the lift due to inclination of the thrust vector. Most of the increase is due to very low pressures induced by the angled jets. Third, the nonuniform jets used in these tests result in lower nondimensional lift loss than the uniform jets having approximately the same mass flow rate. The lift loss, ΔL , produced by the nonuniform jets was about 35% larger than the lift loss due to uniform jets. However, this increase was more than offset by a significant increase of the jet thrust when compared with the uniform jets; hence a decrease in the $\Delta L/T_L$ value. It can also be seen that the nonuniform-jet data points can be brought into "alignment" with the uniform-jet data by moving them to the left, i.e., toward higher R values. This supports the contention that the nonuniform jets behave similarly to the uniform jets having the same mass flow rate but a higher velocity ratio.

Tandem Jets at 60°

The pressure distributions induced by the tandem jet configuration are shown in Figs. 20-23. The distributions are generally characterized by a large negative-pressure region to the sides of the jets, a relatively small positive-pressure region ahead of the front jet and a small region of slightly positive pressures behind the rear nozzle. The upstream portion of the pressure contours, up to about $X/D=+.5$, is essentially determined by the front jet alone. The remaining pressure contours result from the combined influences of both jets. The rear jet is obviously shielded by the front one. The resulting flowfield and surface pressure distribution near the rear jet are very complex and their details could not be resolved with the pressure tap spacing used in these experiments; however, we can identify a few very small, local regions of low pressure/high velocity which may be related to local vortex-type flows. The front/rear jet interaction and the interaction between the jets and the crossflow result in a large projection of negative-pressure area to the sides of rear jet.

The oval-shaped, positive-pressure regions behind the nozzles are likely to be associated with recirculatory flows. We may note that the rear jet, being strongly shielded by the front one, exhausts nearly undeflected until it meets the deflected front jet. Consequently, an extended wake flow may develop behind the rear jet nozzle, involving reversed flow and strong entrainment processes.

Increasing the parameter R in a tandem jet case has similar overall effects on jet-induced surface pressure distributions as those observed in the side-by-side case, i.e., negative-pressure region increases significantly and the upstream positive-pressure region decreases. However, in contrast to the side-by-side case, the negative-pressure region increase is mostly due to an expansion in the lateral direction. The approximate magnitudes of these changes (as R changes from 2.2 to 4), based on the regions enclosed by the lines $\Delta C_p = -.3$ and $\Delta C_p = +.1$ are as follows. First, for uniform velocity profile jets, the negative ΔC_p region increases about 80% and the positive ΔC_p region reduces about 80%. Second, for nonuniform velocity profile jets, the negative ΔC_p region increases about 90% and the positive ΔC_p region decreases almost 90%. The center of the resultant pressure force moves somewhat forward with increasing R .

Comparison of pressure plots for the nonuniform jets with those for the uniform jets indicates, again, trends similar to those produced by an increase in the parameter R . Thus, nonuniform jets generate a larger negative ΔC_p region and a smaller upstream positive ΔC_p region than uniform jets of the same mass flow rate and the same R . At $R=2.2$, the negative ΔC_p area enclosed by the $-.3$ line is about 50% larger with nonuniform jets, while at $R=4$, the increase is about 60%. Most of that increase seems to occur to the sides of the jets which may indicate relatively small changes in the resulting pitching moment.

The positive pressure region which develops along the centerline behind the rear nozzle appears to be more pronounced for the low R case for both uniform and nonuniform jets. It may be recalled here, that for the side-by-side jet configuration, a similar feature (rear positive-pressure region) was observed at low R cases only.

Comparison of the pressure fields induced by the angled ($\theta=60^\circ$) and transverse ($\theta=90^\circ$) jet exhausts reveals the following tentative observations (based on the case of uniform jets with $R=2.2$). First, the negative-pressure region around the 90° jets is significantly larger than for the 60° case (see Figs. 6 and 20). Second, the pressures near the sides of the jet exits are lower for the 60° jets than for the 90° jets which tends to compensate the effect of the reduced negative ΔC_p region for the 60° jets. Third, when the angle changes from 90° to 60° , the center of the negative pressure field moves rearward which leads to an increased nose-up pitching moment on the aircraft. Last, the upstream positive ΔC_p region increases considerably when the jet angle changes from 90° to 60° . This causes a change in the pitching moment having the same trend as the main effect produced by the negative pressure field changes.

Comparison of Pressure Fields for Side-by-Side and Tandem Jets

A general comparison of the surface pressure fields induced by side-by-side and tandem jets indicates some important differences. Tandem jets operated with the same θ , R and exit velocity profile as the side-by-side

jets, induce weaker negative pressure fields, resulting in significantly lower lift losses. This is caused mainly by the fact that the closely spaced rear jet is effectively shielded by the front one and is thus prevented from interacting with the freestream and developing features such as a strong vortex pair which plays an important role in establishing surface pressure field.

Another general characteristic of the tandem jets distinguishing them from the side-by-side jets are the presence of a positive-pressure region in the wake zone and rapid relaxation of the negative pressures behind the jets. The positive-pressure region is likely to be associated with reverse flows which may develop in the wake behind the nearly undeflected rear jet. Rapid relaxation of the downstream pressures may result from strong jet/jet interaction; the ensuing highly intensified turbulent mixing disrupts the vortex pair of the front jet and contributes to a rapid spread and decay of the plume formed from the merged jets. This will be followed by a quick relaxation of surface pressures. Both the positive-pressure region and rapid relaxation of the negative pressures contribute to a decrease in the jet-induced lift loss.

Flowfield Measurements

The velocity vectors in the plane of symmetry of the transversely injected tandem jets with $R=2.2$ are shown in Fig. 24. For the uniform velocity profile jets, the trajectory of the front jet is bent sharply by the oncoming crossflow while the sheltered rear jet rises almost undeflected. The front jet centerline intersects the rear jet at a height of about $Z/D=1.5$. The "combined-jet" centerline, defined as the locus of maximum velocities, penetrates about $4D$ into the freestream. Upward orientation of the velocity vectors beneath the plume is indicative of the presence of a vortex pair.

For the nonuniform jets, the front jet centerline intersects the rear jet at a height of about $Z/D=2$, and the centerline of the "combined jet" penetrates about $5D$ into the freestream. The greater penetration of the nonuniform jets can be readily explained by their greater effective dynamic pressure. The wake of the nonuniform jets decays faster with downstream distance and the velocity vectors below the combined plume are less upward oriented. These observations tend to suggest a stronger turbulent mixing inside the jets and a related weaker vortex pair for the nonuniform jets.

CONCLUDING REMARKS

An experimental study has been conducted to determine surface pressure distributions on a flat plate model with dual side-by-side and tandem jets injected at 90° and 60° angles with jet-to-crossflow velocity ratios of 2.2 and 4. The major objective of the study was to determine the effect of a nonuniform jet velocity profile resembling a practical engine case.

The main conclusions derived from the study are as follows:

1. Nonuniform jets with a high-velocity outer annulus and a low-velocity core induce stronger negative pressure fields than uniform jets

with the same mass flow rate. This effect is mostly due to the higher average dynamic pressure of the nonuniform jets.

2. Changing the injection angle from 90° to 60° results in a moderate (for tandem jets) to significant (for side-by-side jets) increase of the induced negative pressures and, hence, in increased lift loss, even though the surface area influenced by the jets tends to reduce as the angle decreases.

3. Side-by-side jets result in significant nondimensional jet-induced lift losses, $\Delta L/T_L$, which are comparable to or greater than the lift losses reported for single jets.

4. Nondimensional lift losses induced by nonuniform jets are lower than lift losses due to uniform jets.

5. Nonuniform jets induce larger nose-up pitching moments than the uniform jets with the same R , θ and jet configuration.

6. Closely spaced tandem jets induce considerably lower lift losses than side-by-side jets.

7. Pressure fields induced by tandem jets feature a positive-pressure region in the wake flow and a rapid relaxation of the negative pressures behind the jets. Both these effects contribute to a decrease in the jet-induced lift loss.

8. For all the configurations tested, the effect of R was the same as previously documented in literature. As R is increased (from 2.2 to 4), both the surface area influenced by the jets and the resultant negative pressure force increase. However, this trend is not expected to continue at higher R values. On the basis of physical arguments presented in this paper it is suggested that, at least with 90° injection, the trend will be reversed when R increases above about 8.

Simple physical explanations are offered for the main trends and effects observed in these experiments. The pronounced effects of dual jet configuration, jet injection angle and exit velocity profile upon the induced aerodynamic loads point to a need for a more systematic investigation of the respective effects. In particular, it is recommended that experiments are extended over a wider range of injection angle ($\theta = 45^\circ - 105^\circ$), higher velocity ratios, and other jet exit velocity profiles. They also should include investigation of the effects of swirl and initial jet turbulence.

ACKNOWLEDGEMENTS

The authors wish to express their sincere gratitude to George Aoyagi from NASA Ames who made it possible for us to receive the necessary instrumentation thus contributing greatly to our research. He was also most helpful in providing us with information and advice concerning selection of the jet profiles and pressure measuring techniques.

REFERENCES

1. Volger, R.D., "Surface Pressure Distributions Induced on a Flat Plate by a Cold Air Jet Issuing Perpendicularly from the Plate and Normal to a Low-Speed Free-Stream Flow," NASA TN D-1629, 1963.
2. Bradbury, L.J.S. and Wood, M.N., "The Static Pressure Distributions Around a Circular Jet Exhausting Normally From a Plane Wall Into an Airstream," C.P. No. 822, Brit. A.R.C., 1965.
3. Margason, R.J., "Jet-Induced Effects in Transition Flight," Conference on V/STOL and STOL Aircraft, NASA SP-116, 1966, pp. 177-189.
4. Margason, R.J., "Review of Propulsion-Induced Effects on Aerodynamics of Jet/STOL Aircraft," NASA TN D-5617, 1970.
5. Fearn, R.L. and Weston, R.P., "Induced Pressure Distribution of a Jet in a Crossflow," NASA TN D-7916, 1975.
6. Vogler, R.D., "Interference Effects of Single and Multiple Round or Slotted Jets on a VTOL Model in Transition," NASA TN D-2380, 1964.
7. Fricke, L.B., Wooler, P.T. and Ziegler, H., "A Wind Tunnel Investigation of Jets Exhausting Into a Crossflow," AFFDL-TR-70-154, Vols. I-IV, U.S. Air Force, December 1970.
8. Schetz, J.A., Jakubowski, A.K. and Aoyagi, K., "Surface Pressures on a Flat Plate with Dual Jet Configurations," Journal of Aircraft, Vol. 21, No. 7, 1984, pp. 484-490.
9. Perkins, S.C., Jr. and Mendenhall, M.R., "A Study of Real Jet Effects on the Surface Pressure Distribution Induced by a Jet in a Crossflow," NASA CR-166150, 1981.
10. Kuhlman, J.M., Ousterhout, D.S. and Warcup, R.W., "Experimental Investigation of Effect of Jet Decay Rate on Jet-Induced Pressures on a Flat Plate," NASA CR-2979, 1978.
11. Ziegler, H. and Wooler, P.T., "Analysis of Stratified and Closely Spaced Jets Exhausting into a Crossflow," NASA CR-132297, 1973.
12. Marchman, J.F., "Wind Tunnel Lab Manual," Dept. of Aerospace and Ocean Engineering, Virginia Polytechnic Institute and State University, Blacksburg, VA.
13. Abramovich, G.N., "The Theory of Turbulent Jets," MIT Press, Cambridge, MA, 1960.

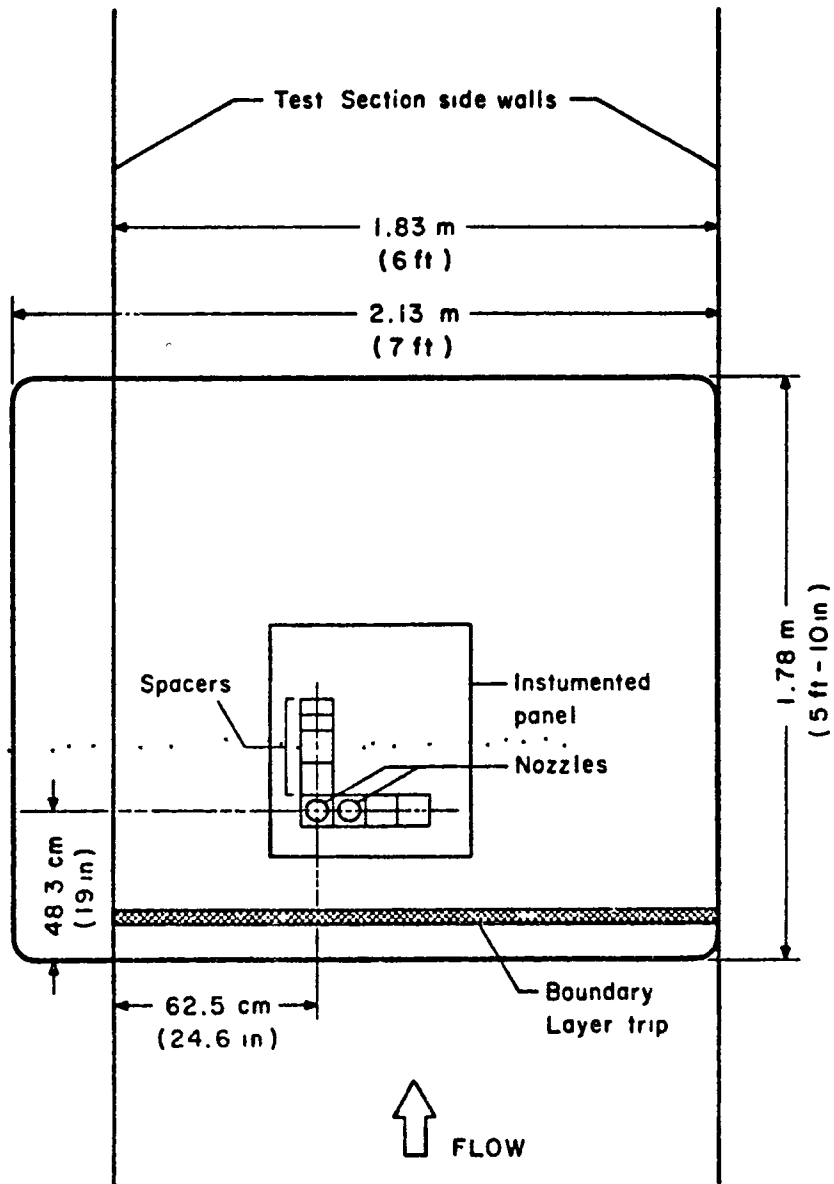


Fig. 1 Flat Plate Model

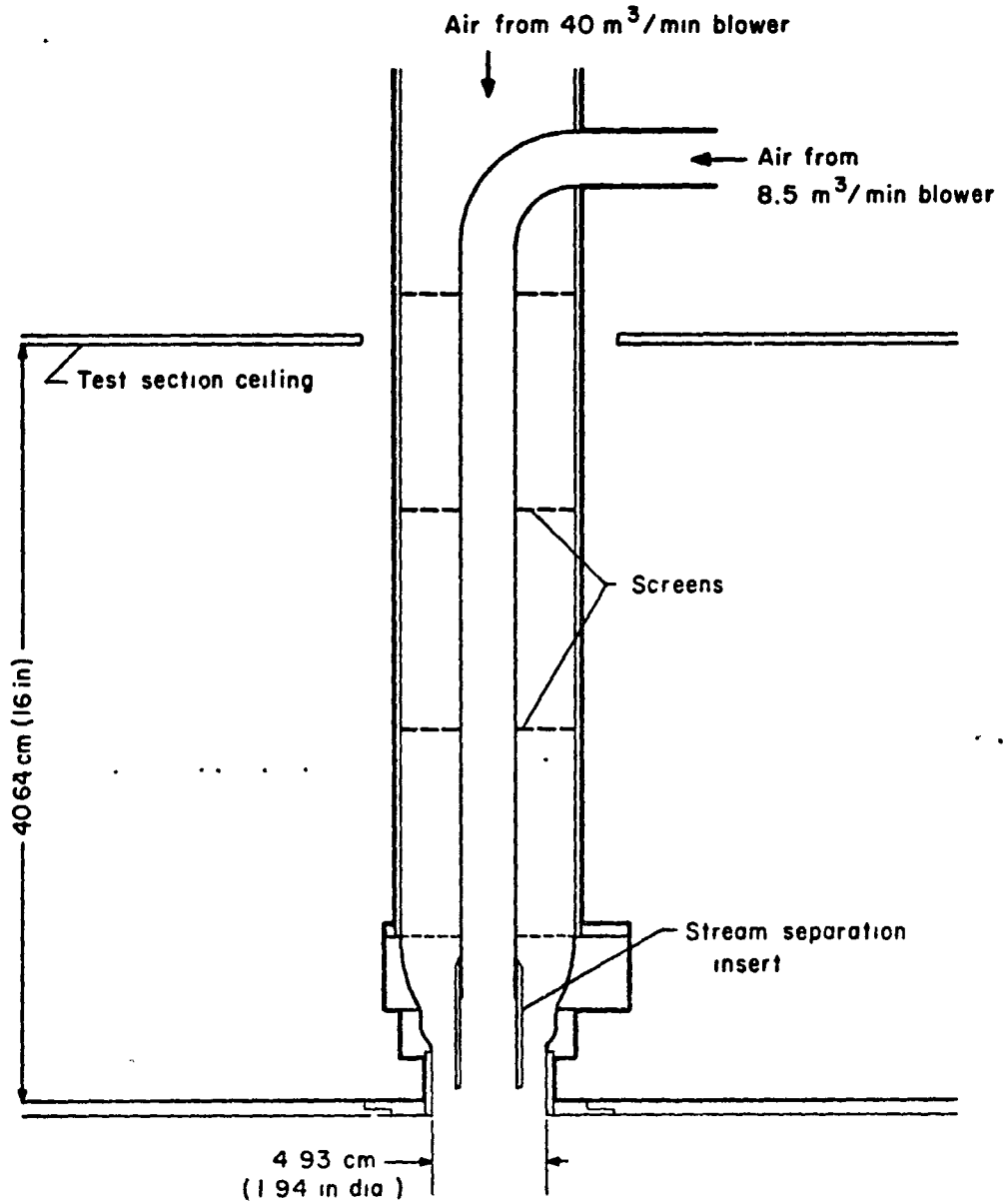
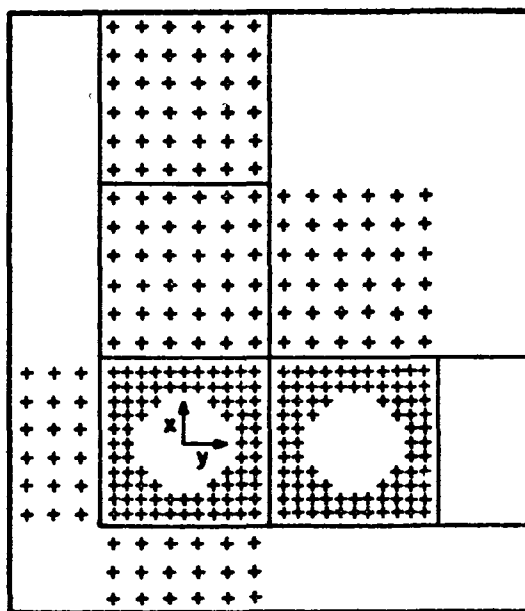
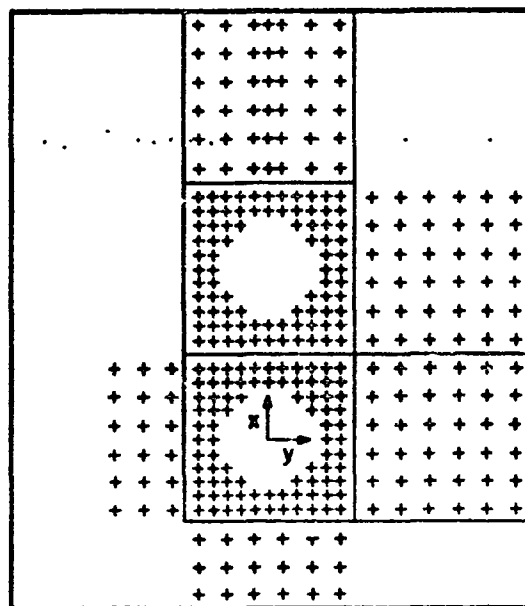


Fig. 2 Cross-Sectional View of Nozzle Assembly

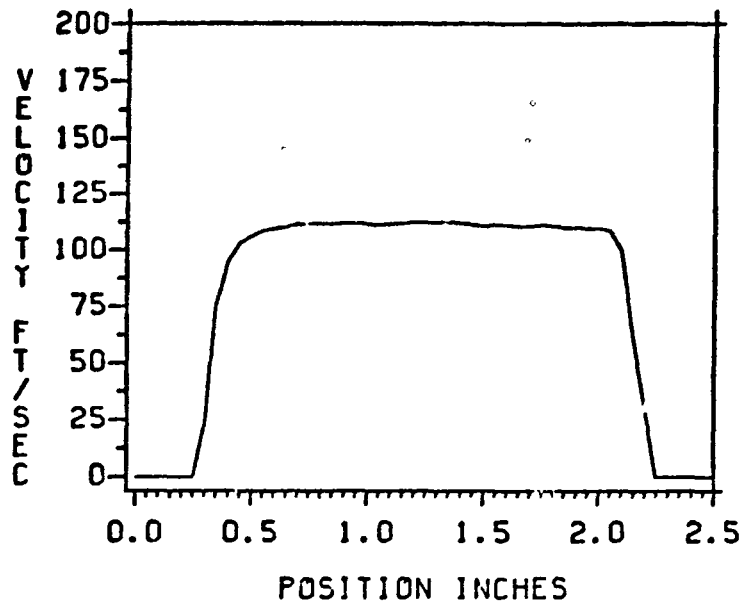


(a) Side-by-Side Configuration

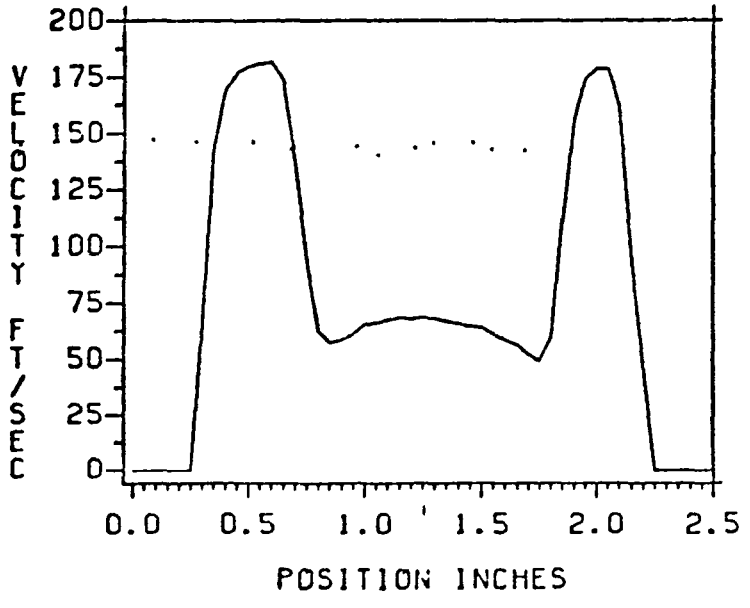


(b) Tandem Configuration

Fig. 3 Plate Pressure Tap Layouts

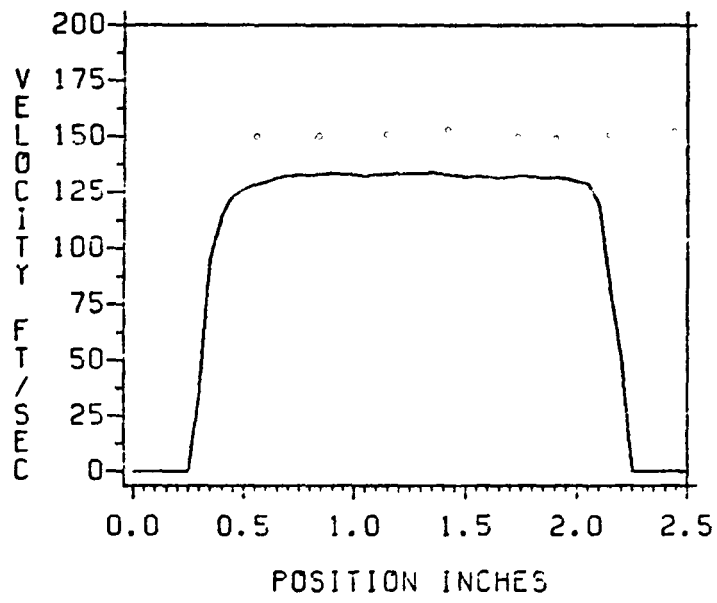


Uniform Exit Profile

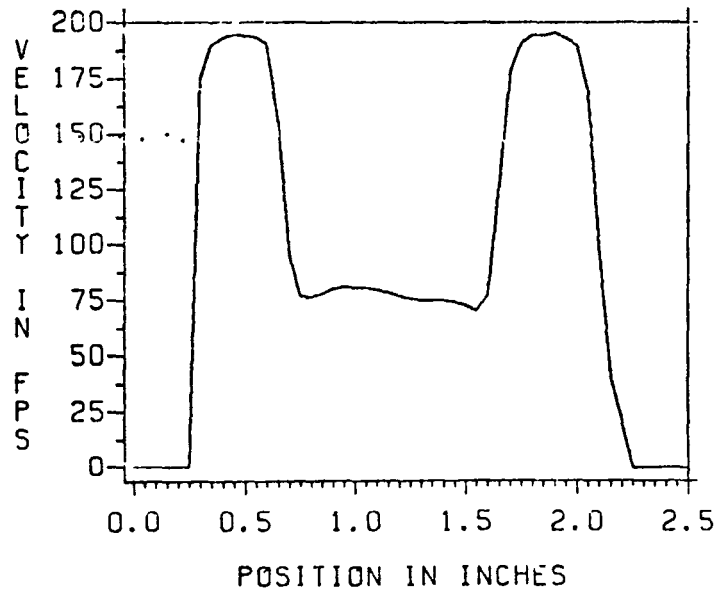


Nonuniform Exit Profile

Fig. 4a Exit Velocity Profiles of 90° Jets.
Pitot-Static Probe Tip 1.6 mm
(1/16 in) from Nozzle Exit

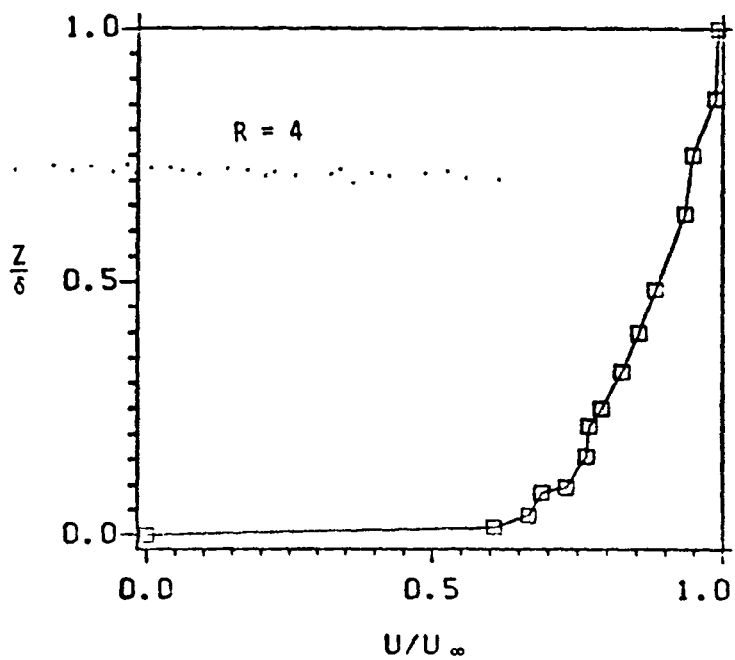
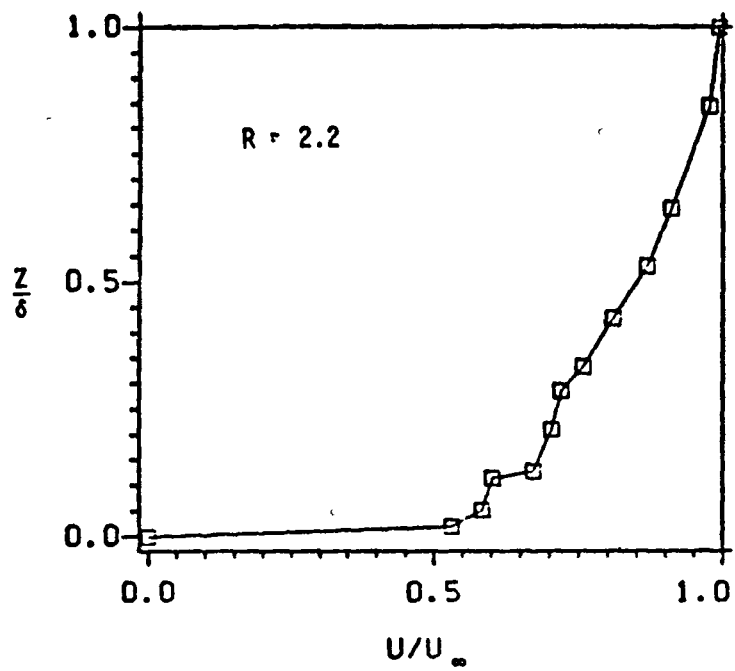


Uniform Exit Profile



Nonuniform Exit Profile

Fig. 4b Exit Velocity Profiles of 60° Jets.
Pitot-Static Probe Tip 1.6 mm
(1/16 in) from Nozzle Exit

Fig. 5 Boundary Layer Profiles, 90° Jets

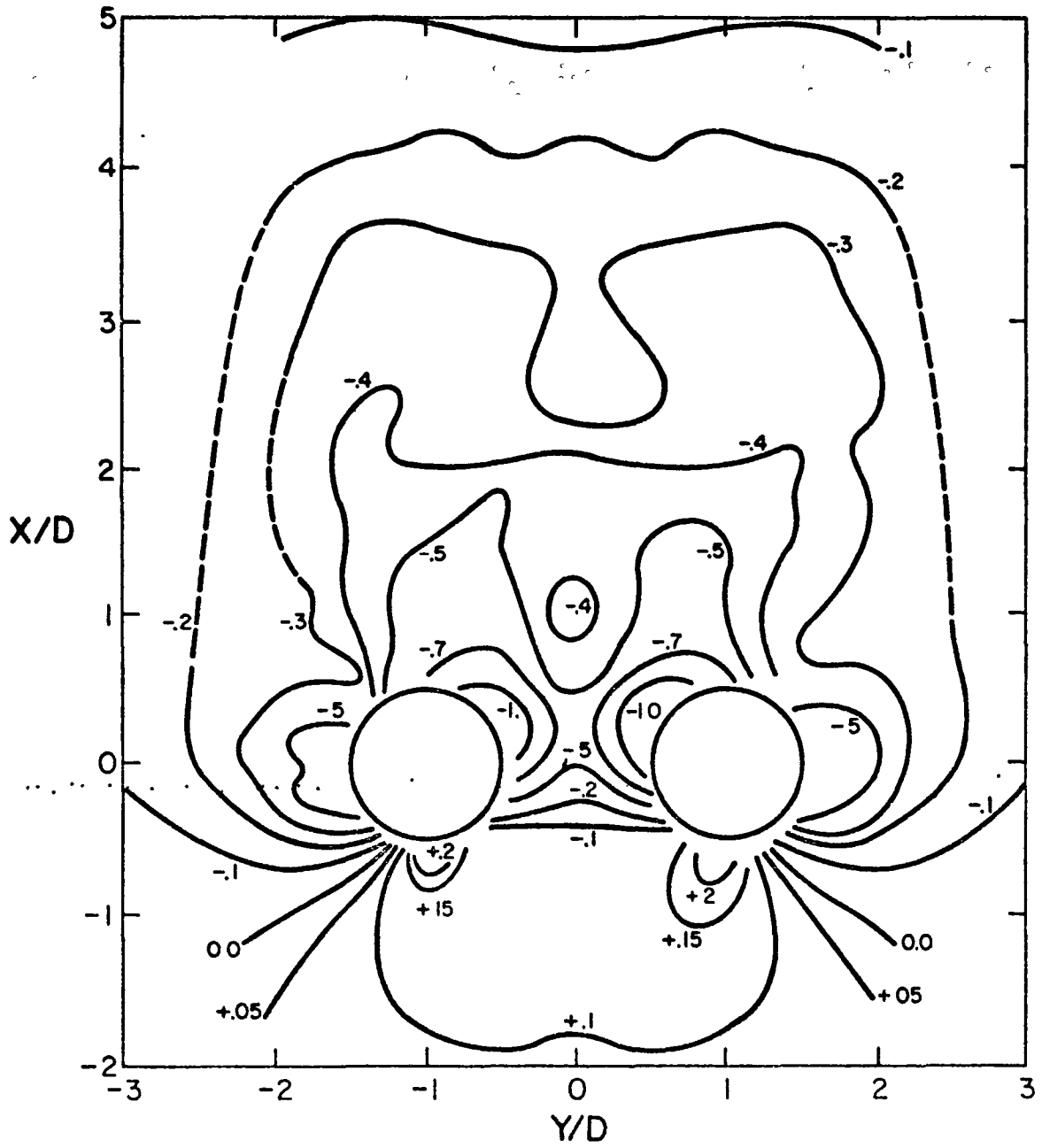


Fig 6 Induced Pressure Distribution (C_p)
 Side-by-Side Jets, Uniform Exit Profile,
 $\theta = 90^\circ$, $R = 2.2$

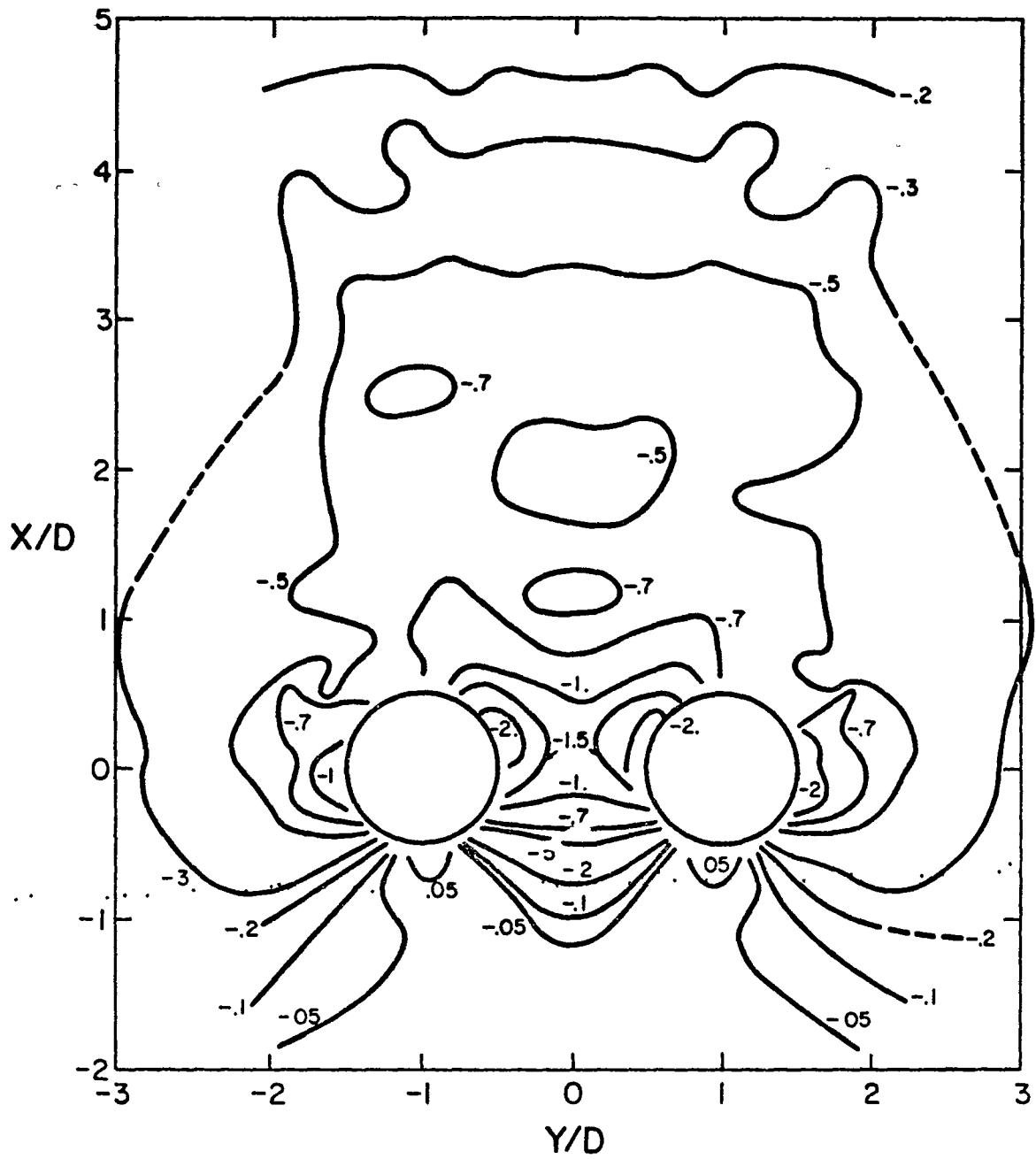


Fig 7 Induced Pressure Distribution (C_p)
 Side-by-Side Jets, Uniform Exit Profile,
 $\theta = 90^\circ$, $R = 4$

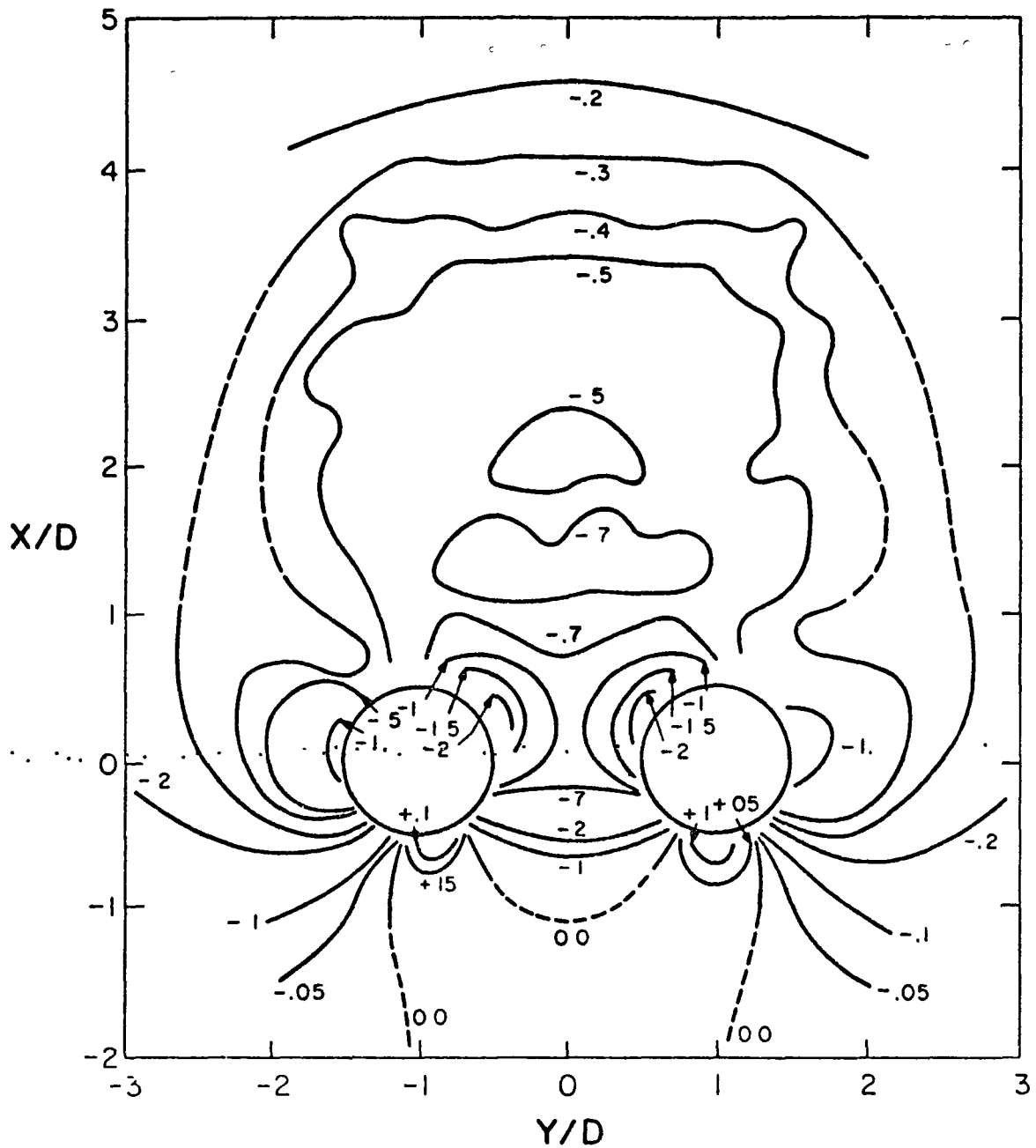


Fig. 8 Induced Pressure Distribution (ΔC_p):
Side-by-Side Jets, Nonuniform Exit Profile, $\theta = 90^\circ$, $R = 2.2$

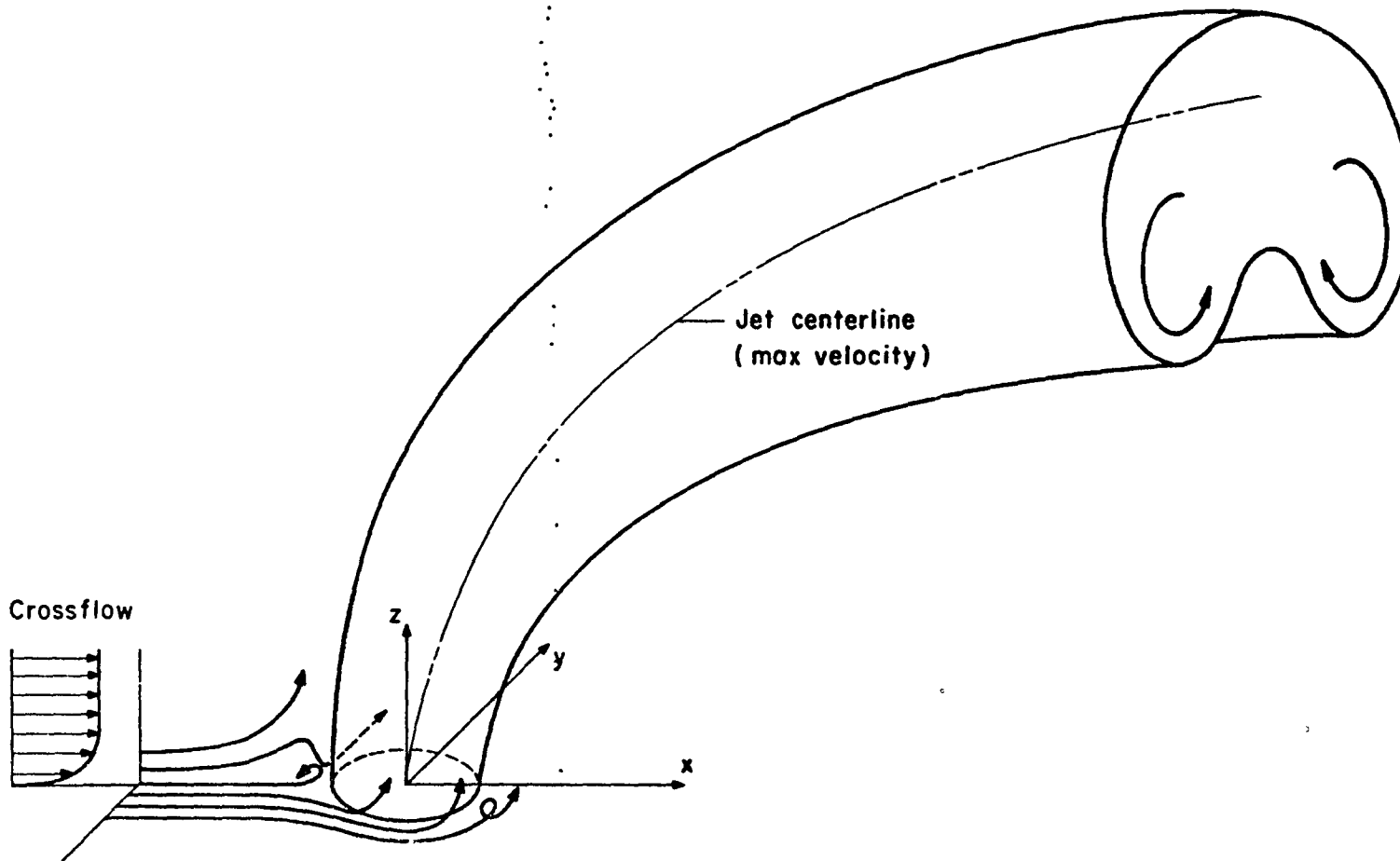


Fig. 10 Schematic View of a Jet Exiting at $\theta = 90^\circ$ into a Crossflow

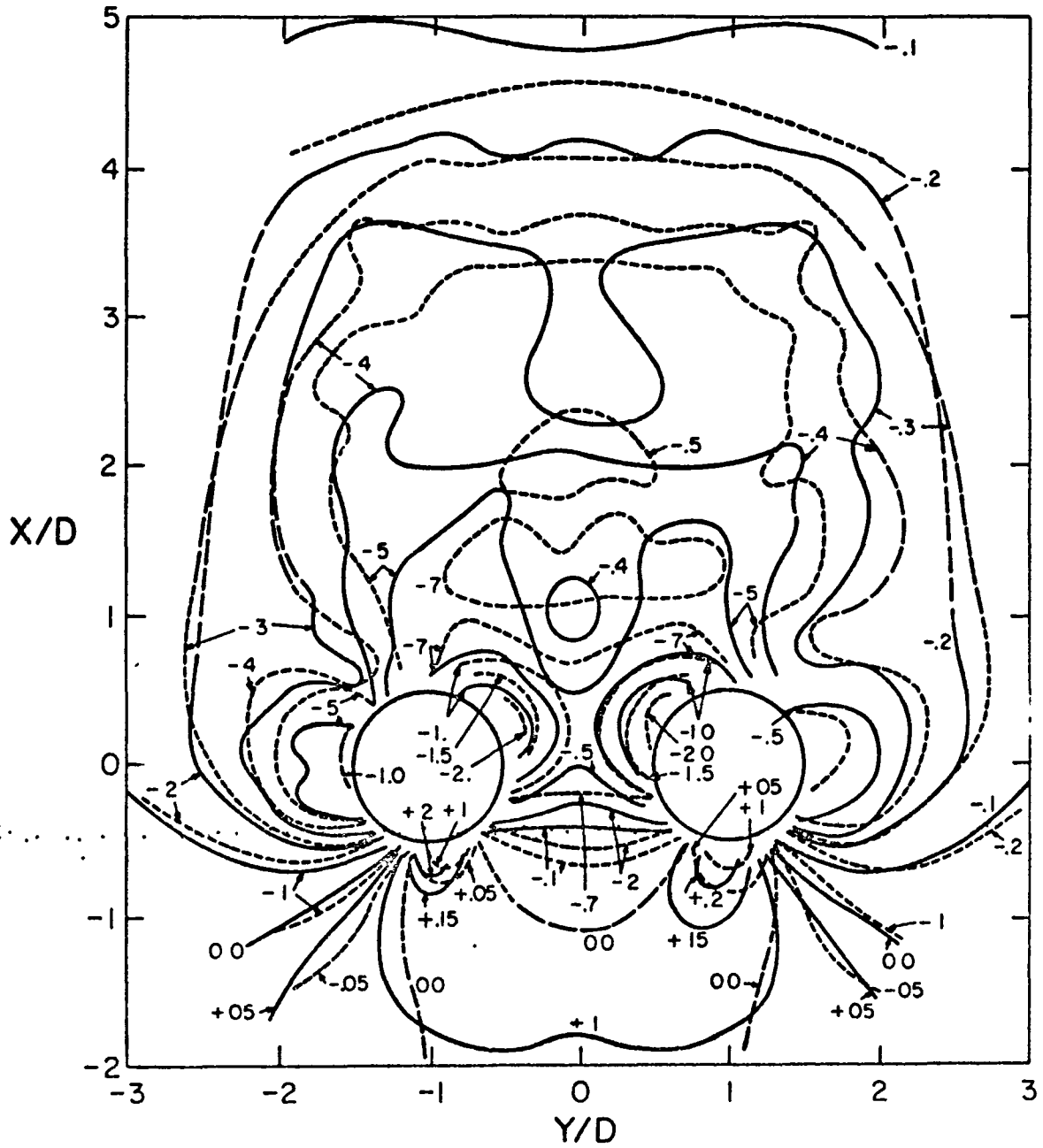


Fig. 11 Effect of Exit Velocity Profile on Induced Pressure Distribution (C_p) for Side-by-Side Jets, $\theta = 90^\circ$, $R = 2.2$.

————— Uniform Exit Profile
 - - - - - Nonuniform Exit Profile

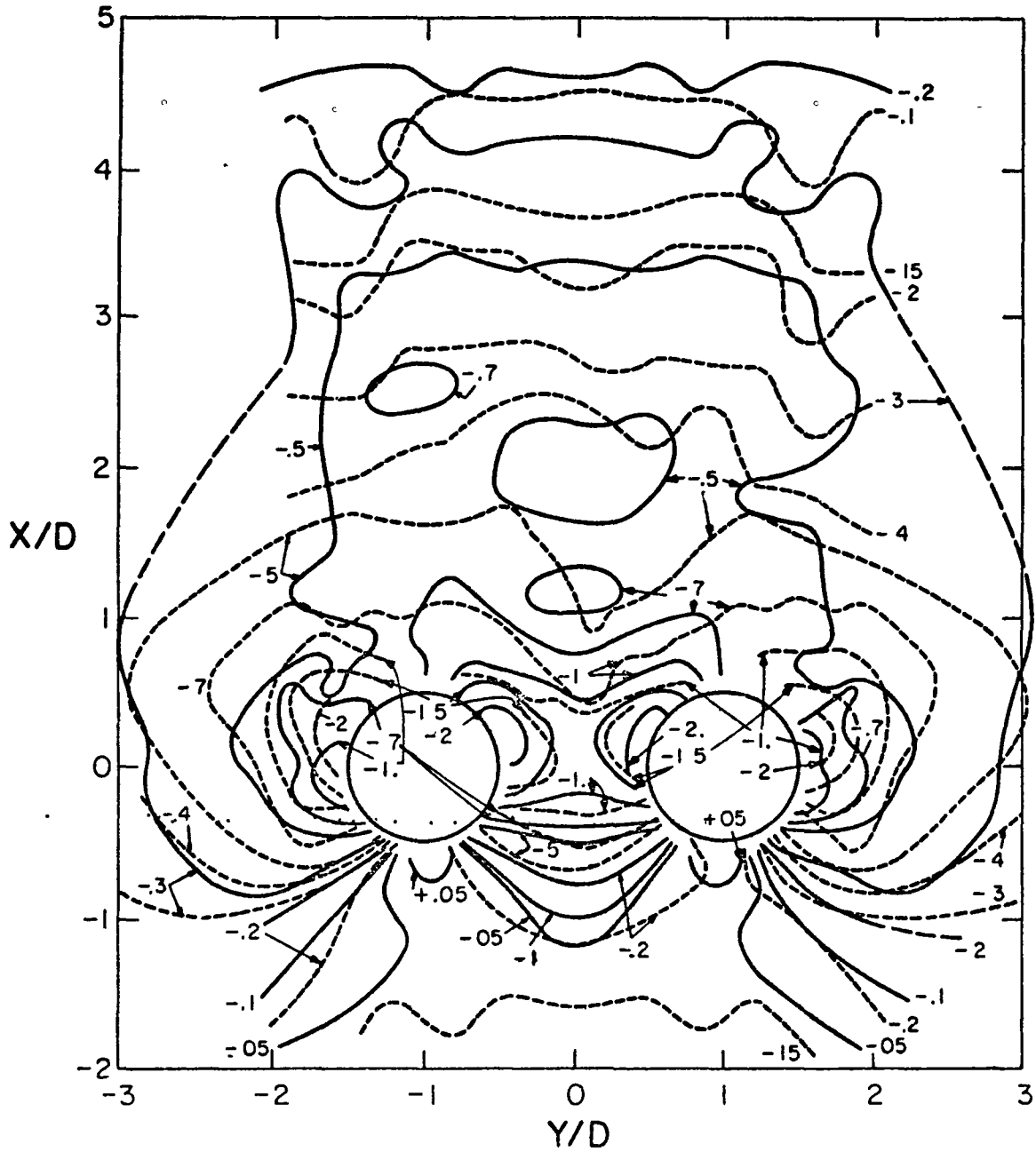


Fig. 12 Effect of Exit Velocity Profile on Induced Pressure Distribution (ΔC_p) for Side-by-Side Jets, $\theta = 90^\circ$, $R = 4$:

————— Uniform Exit Profile
 - - - - - Nonuniform Exit Profile

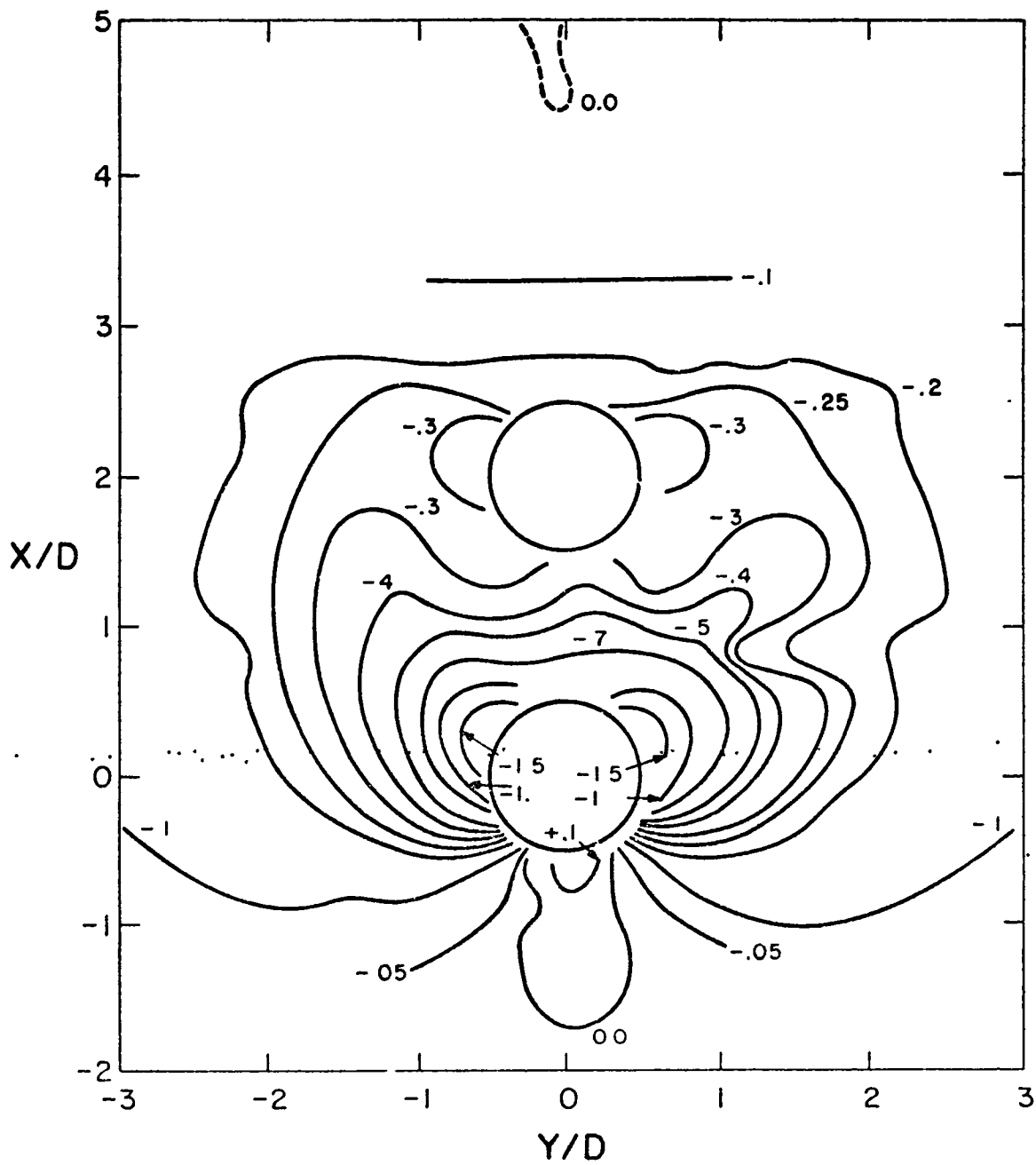


Fig. 13 Induced Pressure Distribution (ΔC_p):
Tandem Jets, Uniform Exit Profile, $\theta = 90^\circ$, $R = 2.2$

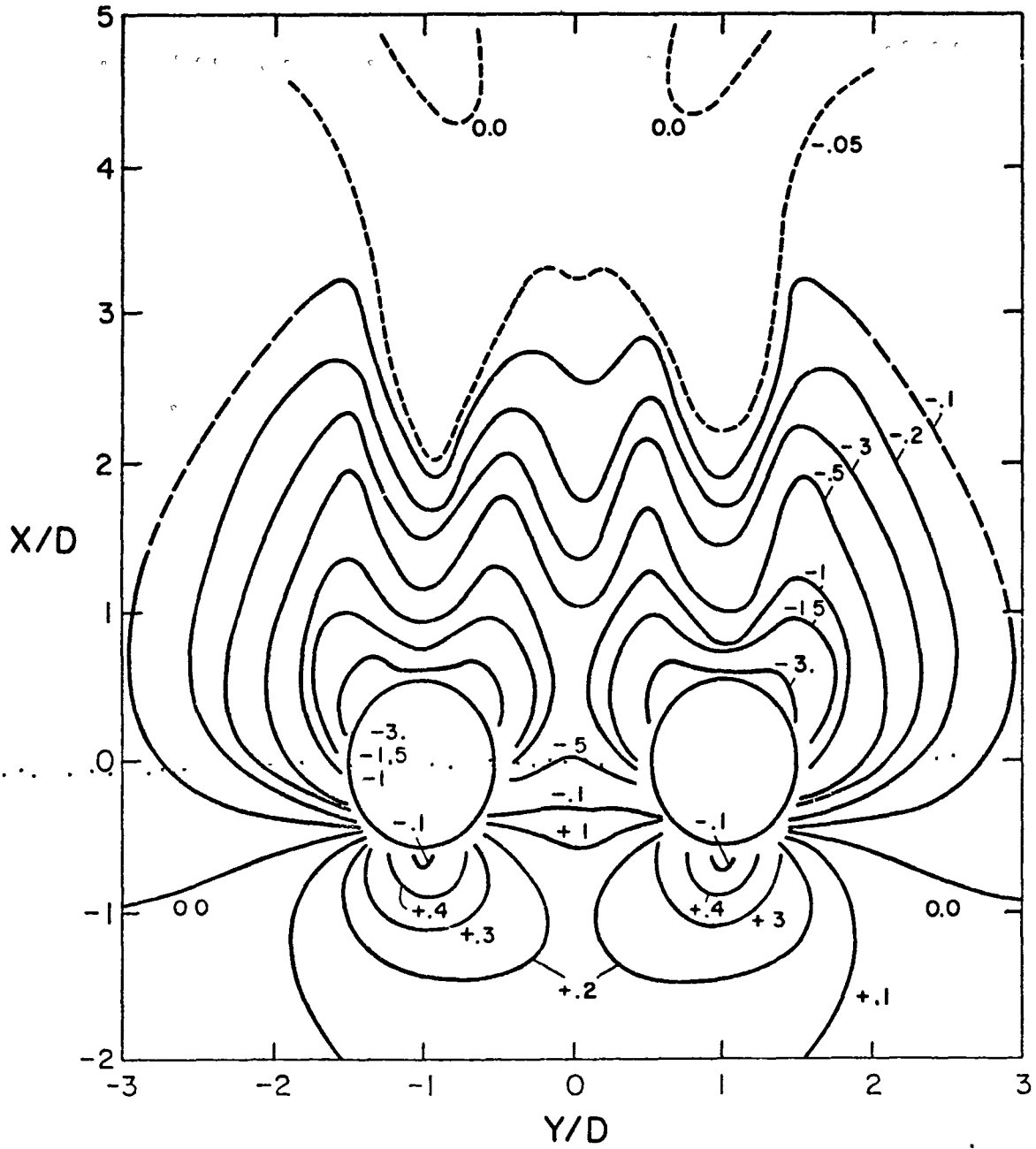


Fig. 14 Induced Pressure Distribution (ΔC_p):
Side-by-Side Jets, Uniform Exit Profile, $\theta = 60^\circ$, $R = 2.2$

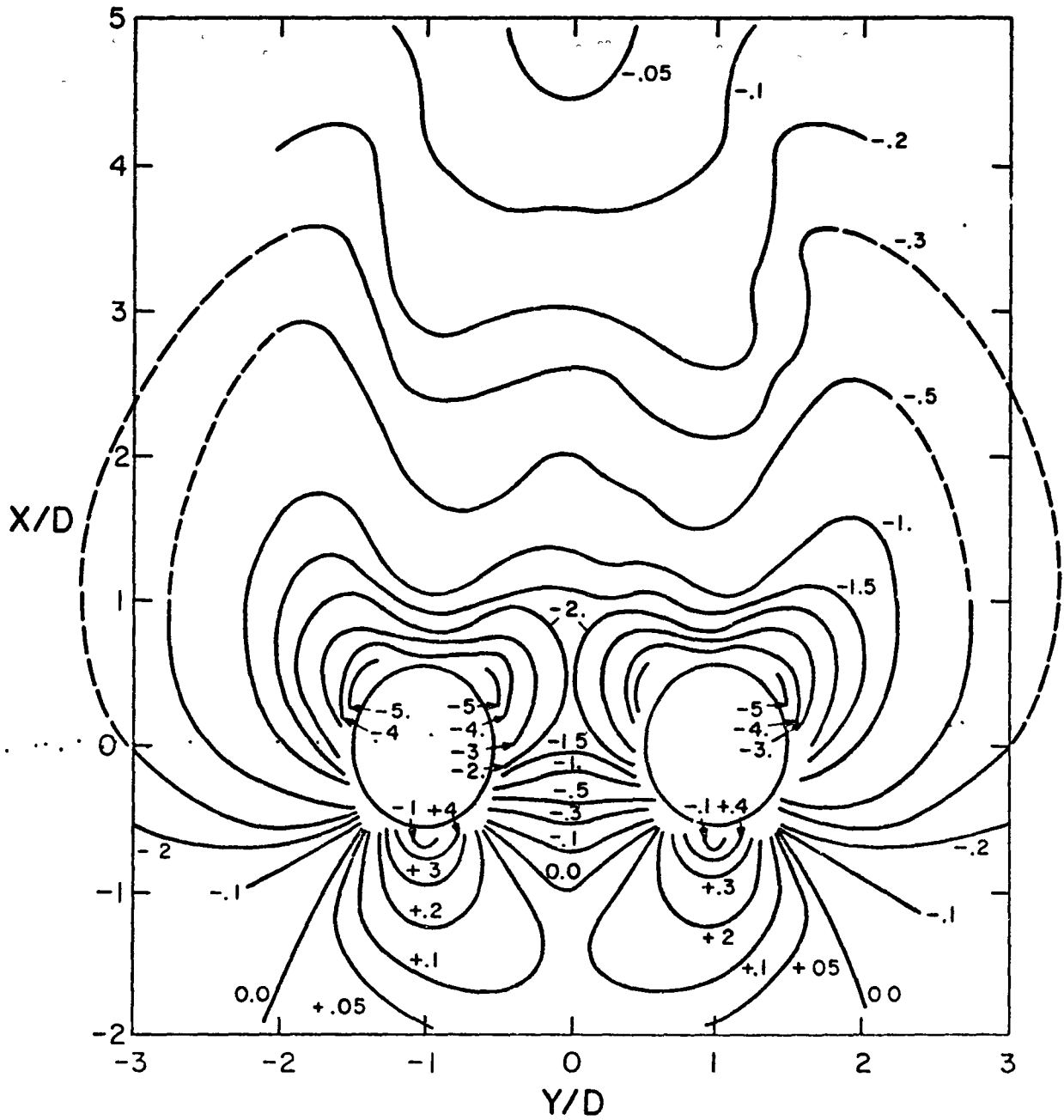


Fig. 15 Induced Pressure Distribution (ΔC_p):
Side-by-Side Jets, Uniform Exit Profile, $\theta = 60^\circ$, $R = 4$

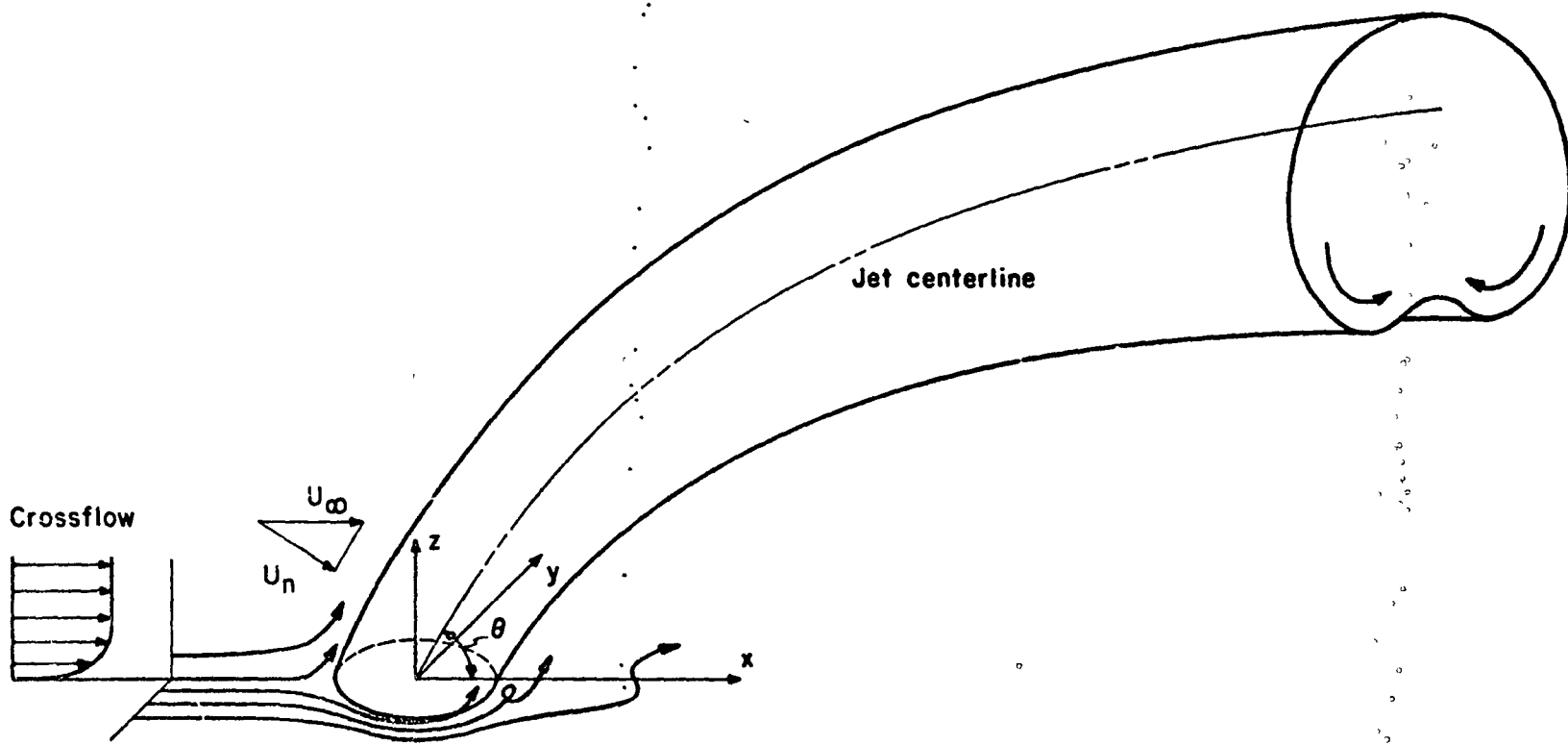


Fig. 16 Schematic View of a Jet Exiting at $\theta = 60^\circ$ into a Crossflow

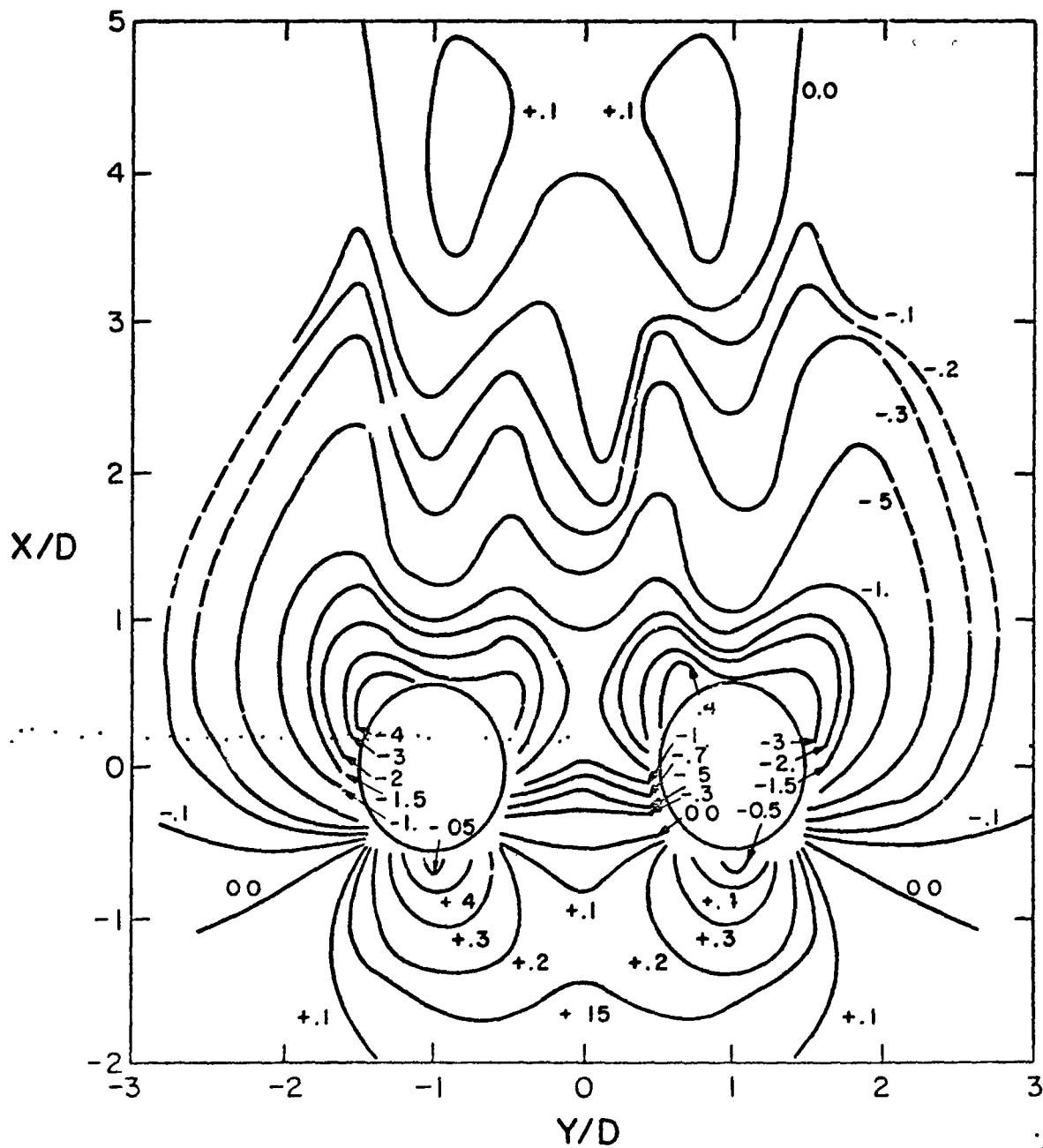


Fig. 17 Induced Pressure Distribution (ΔC_p):
Side-by-Side Jets, Nonuniform Exit Profile, $\theta = 60^\circ$, $R = 2.2$

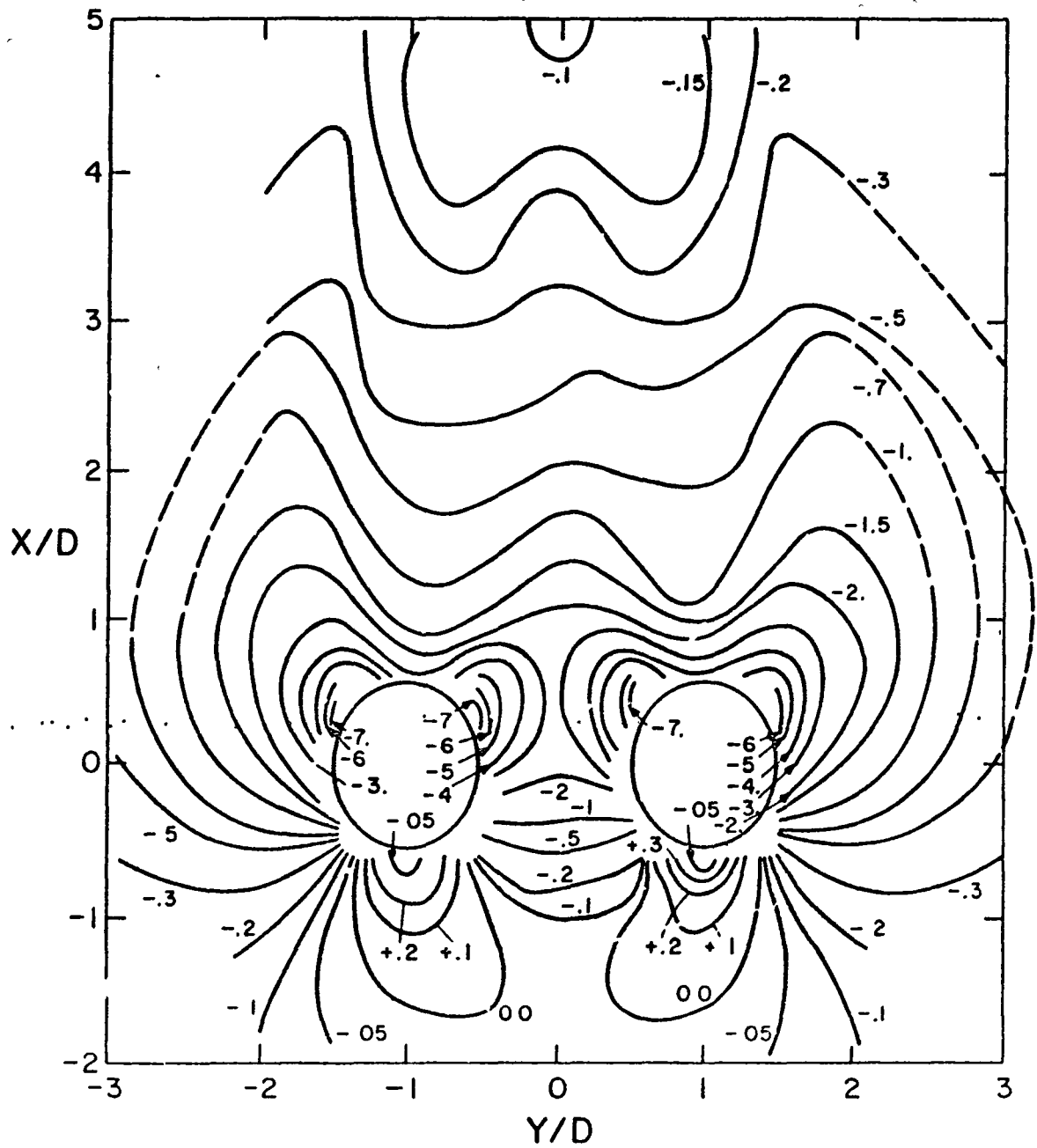


Fig. 18 Induced Pressure Distribution (ΔC_p):
Side-by-Side Jets, Nonuniform Exit Profile, $\theta = 60^\circ$, $R = 4$

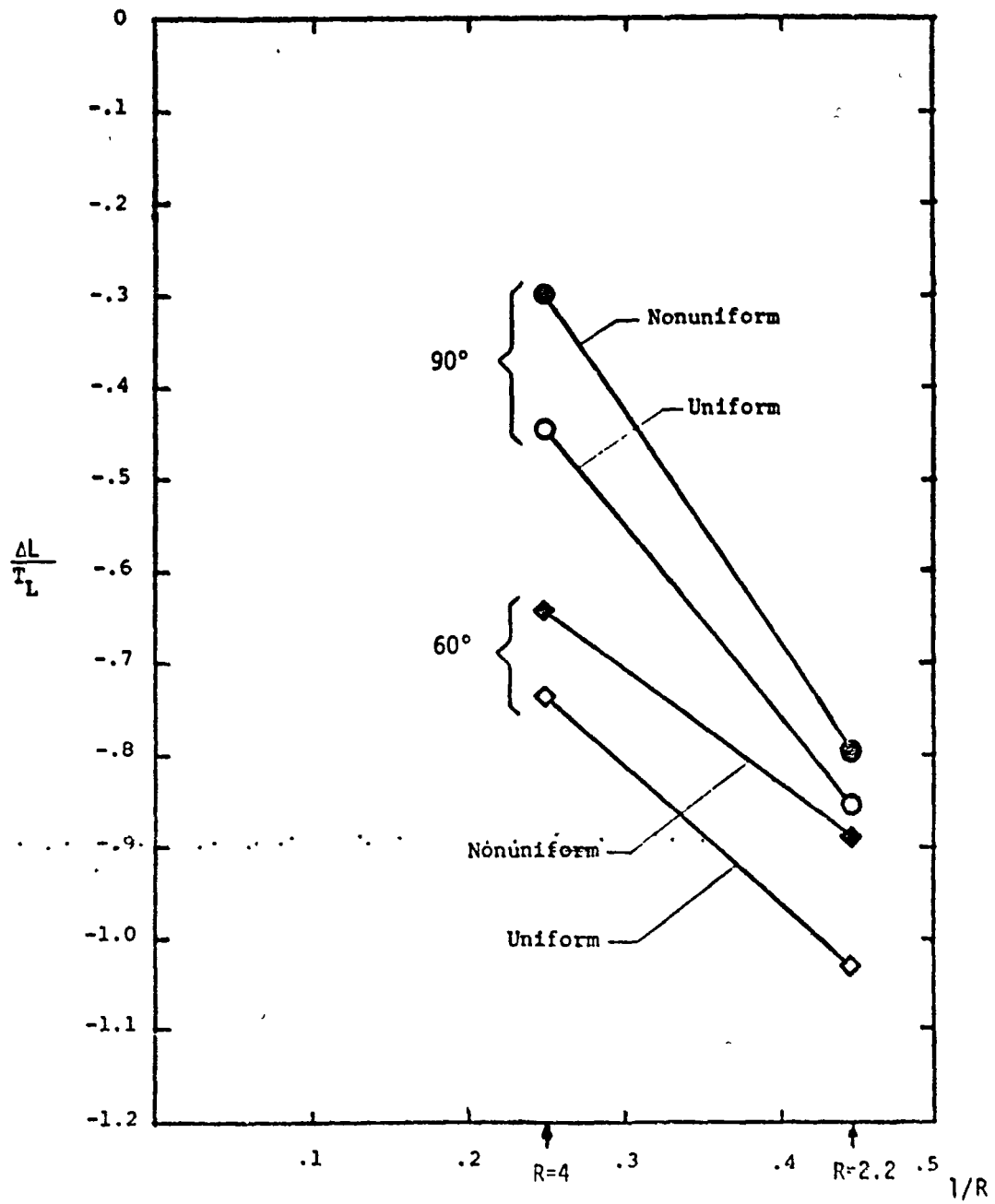


Fig. 19 Nondimensional Jet-Induced Lift Loss for Side-by-Side Jets. Two Nozzle Diameter Spacing between Nozzles.

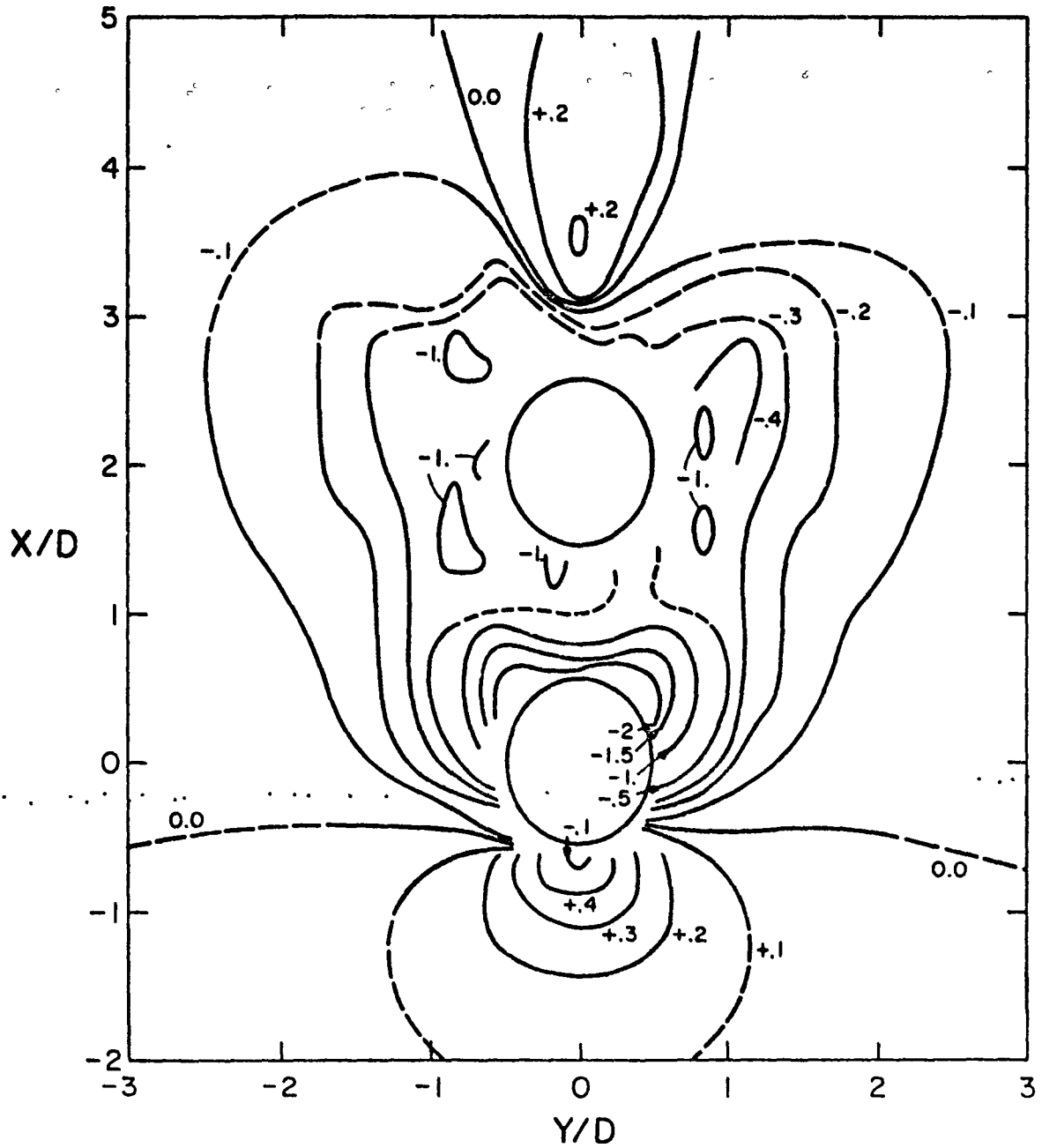


Fig. 20 Induced Pressure Distribution (ΔC_p):
Tandem Jets, Uniform Exit Profile, $\theta = 60^\circ$, $R = 2.2$

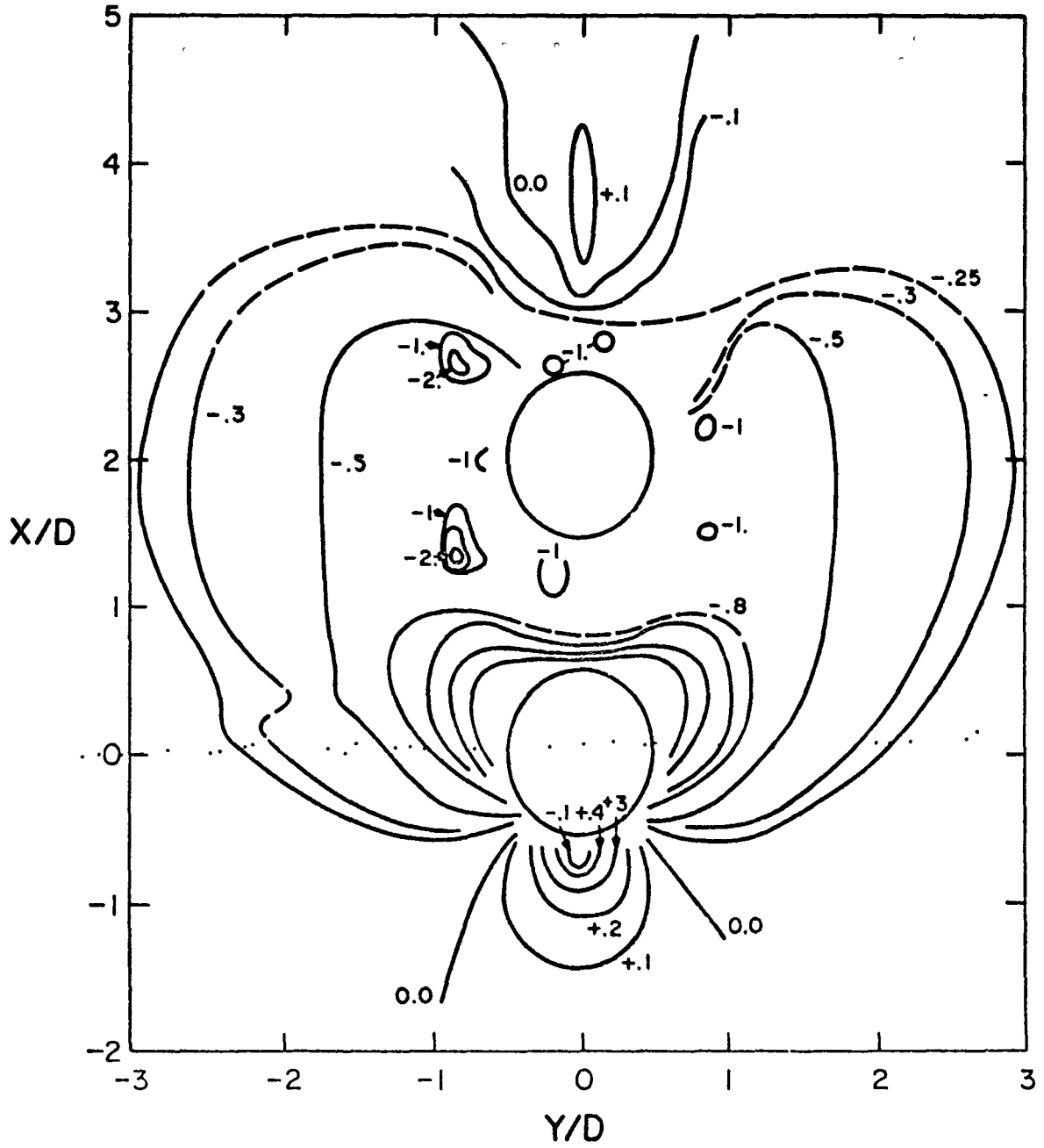


Fig. 21 Induced Pressure Distribution (ΔC_p):
Tandem Jets, Uniform Exit Profile, $\theta = 60^\circ$, $R = 4$

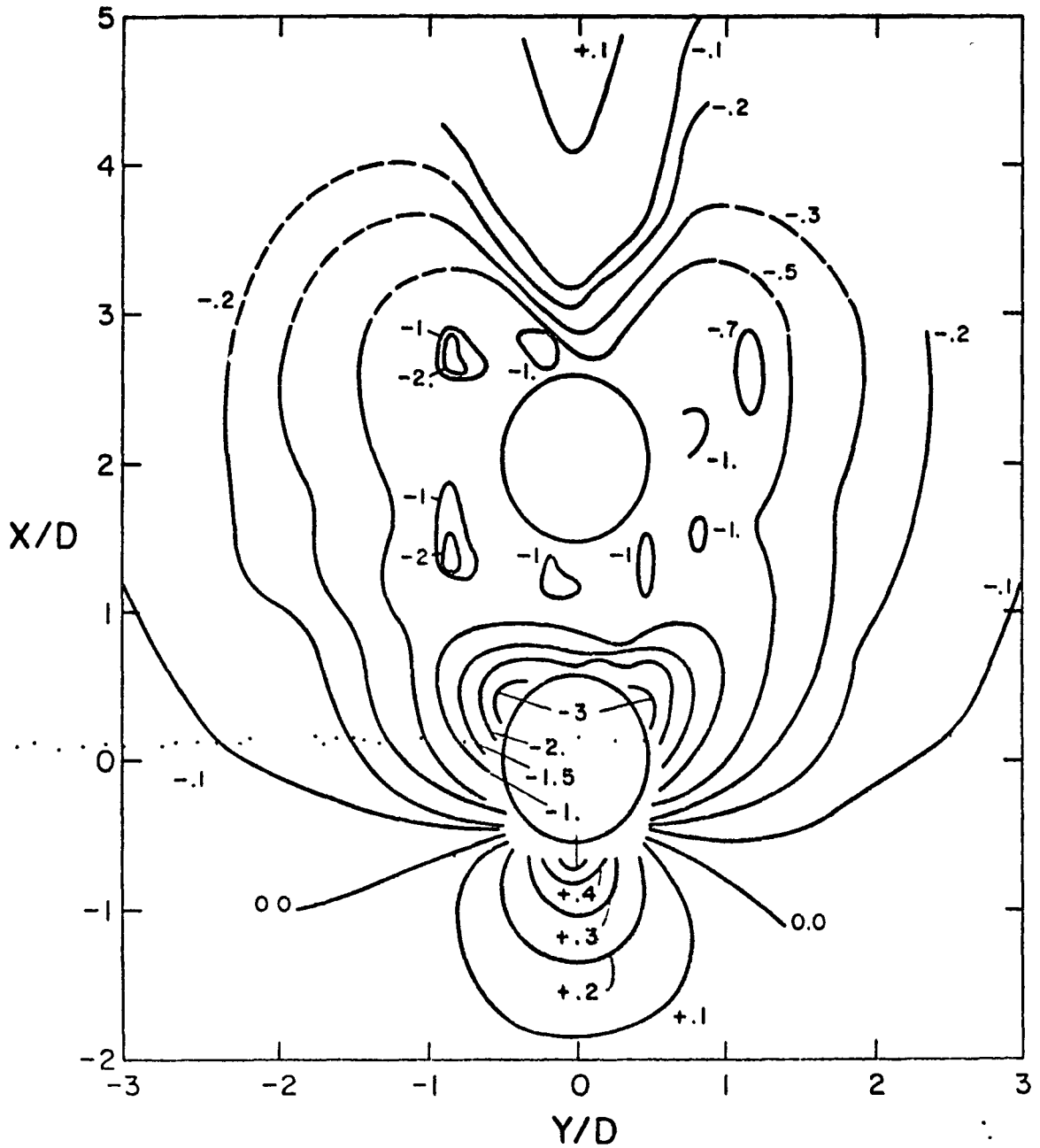


Fig. 22 Induced Pressure Distribution (ΔC_p):
Tandem Jets, Nonuniform Exit Profile, $\theta = 60^\circ$, $R = 2.2$

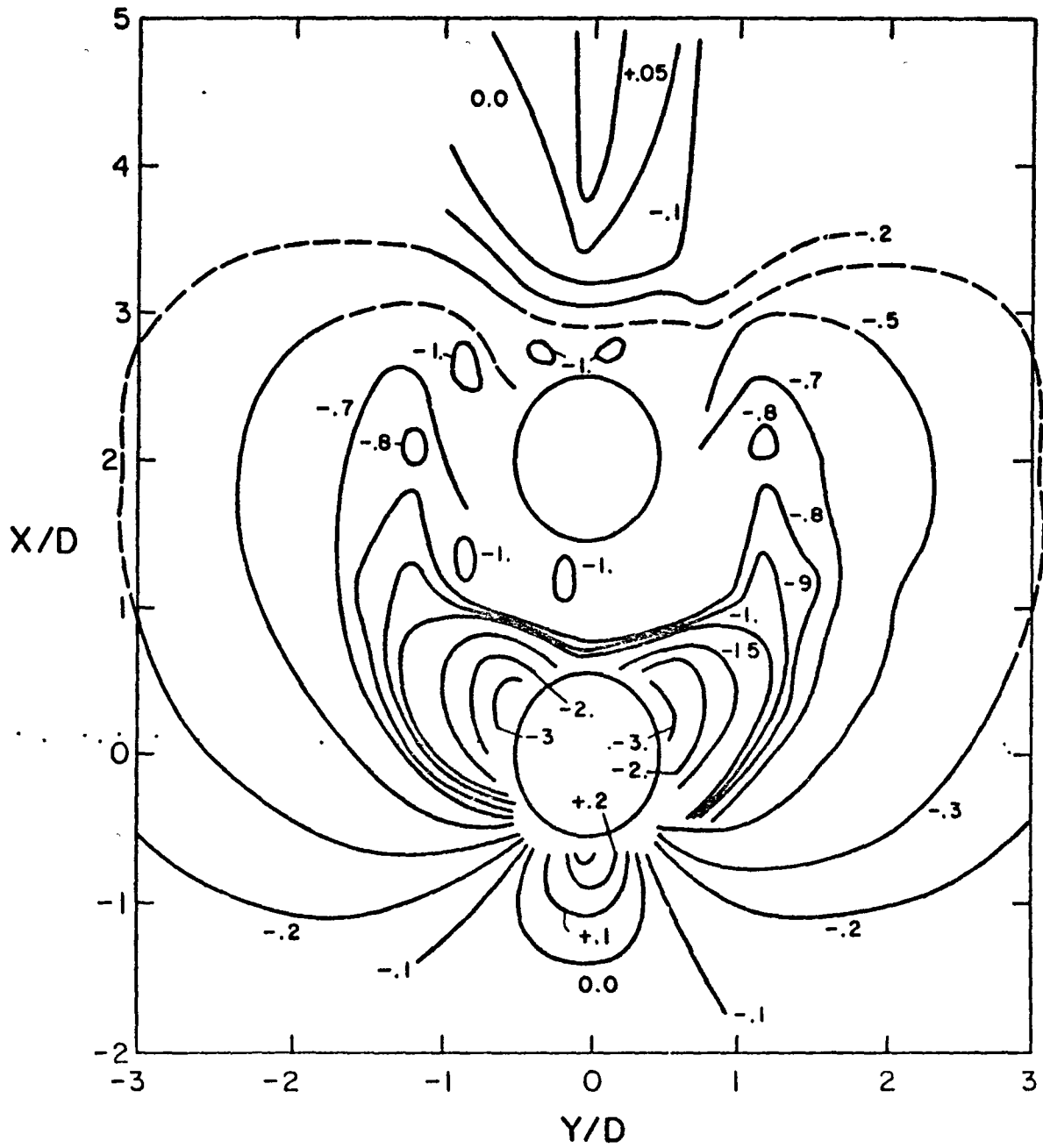


Fig. 23 Induced Pressure Distribution (ΔC_p):
Tandem Jets, Nonuniform Exit Profile, $\theta = 60^\circ$, $R = 4$

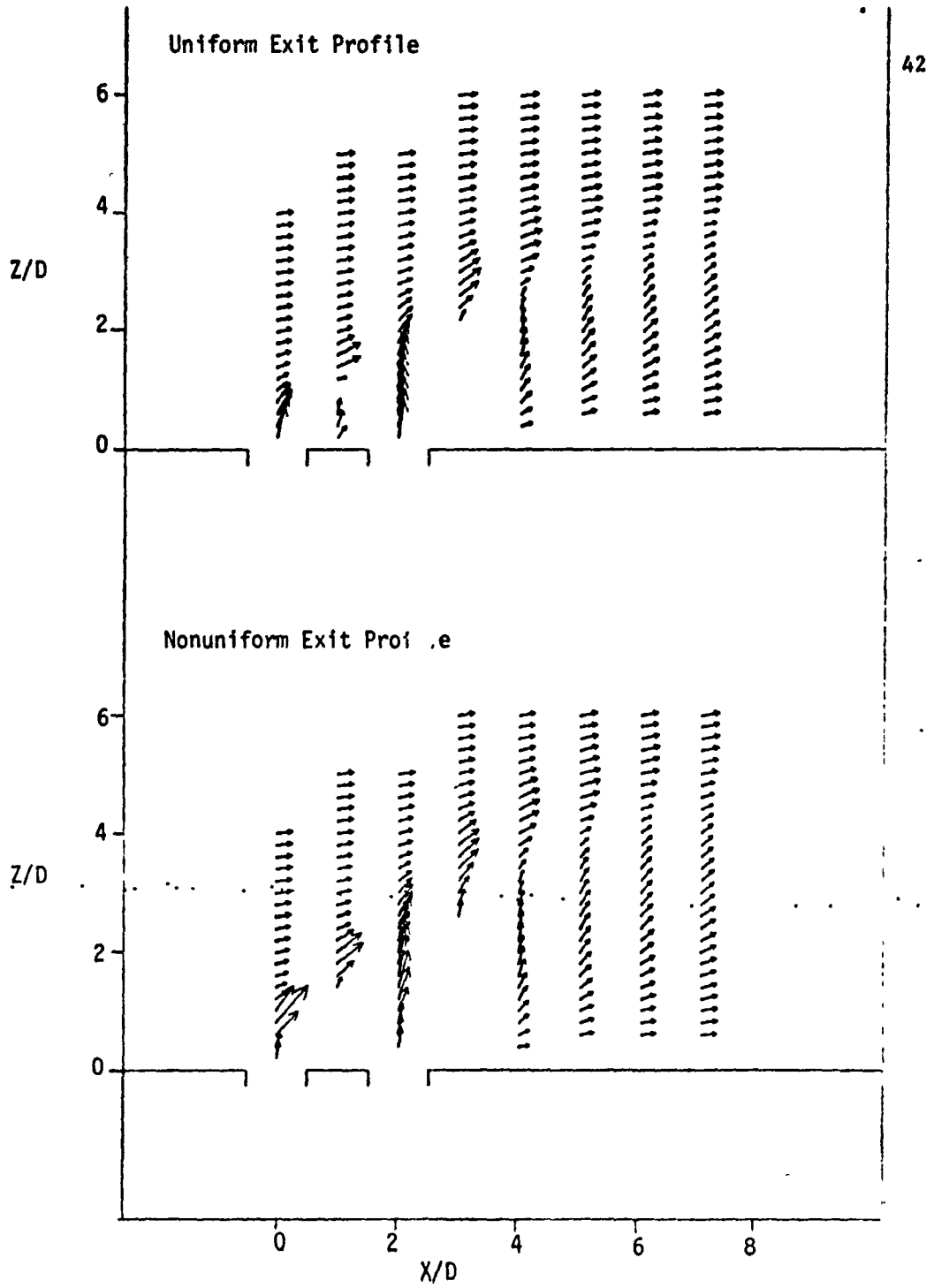


Fig. 24 Velocity Vector Plots:
Tandem Jets, $\theta = 90^\circ$, $R = 2.2$

APPENDIX A

COMPARISON OF MACHINE AND HAND-MADE PRESSURE CONTOURS

Figures A1-A3 compare pressure contours traced out by computer with contours obtained by hand plotting. The computer plots were generated by the Cal Comp General Purpose Contouring Programs. Spacing of the grid points at which the pressure magnitudes and gradients were established, was varied between 0.1 D and 0.5 D. The plots generated with grid spacing of 0.25 D were judged to be the most adequate, and they are shown in Figs. A1-A3. The hand-made contours were traced out on the computer generated layouts of the numerical pressure data.

From Figs. A1-A3 it can be seen that computer tracing worked quite well in regions where the density of input data points (compare Fig. 3) was sufficiently large to handle local pressure gradients. Near the inner (i.e., nozzle exits) and outer boundaries, as well as in regions containing rapid pressure changes concentrated in small areas, the computer plotting failed to produce satisfactory contours. While the machine plots were judged to be of inadequate accuracy for handling all the data of these experiments, it is expected that sufficient accuracy can be obtained in future applications provided that the two following conditions can be met:

1. The surface area covered by the input data must be increased considerably; such area should be at least 60 times larger than the exit nozzle area. This would allow to plot accurately the negative-pressure contours down to, at least, ΔC_p values of $-.2$.
2. The density of pressure input data near the nozzle exits should be increased; the spacing between the pressure taps next to the nozzles should be as small as possible (3-4 mm (0.12 - 0.16 in.)).

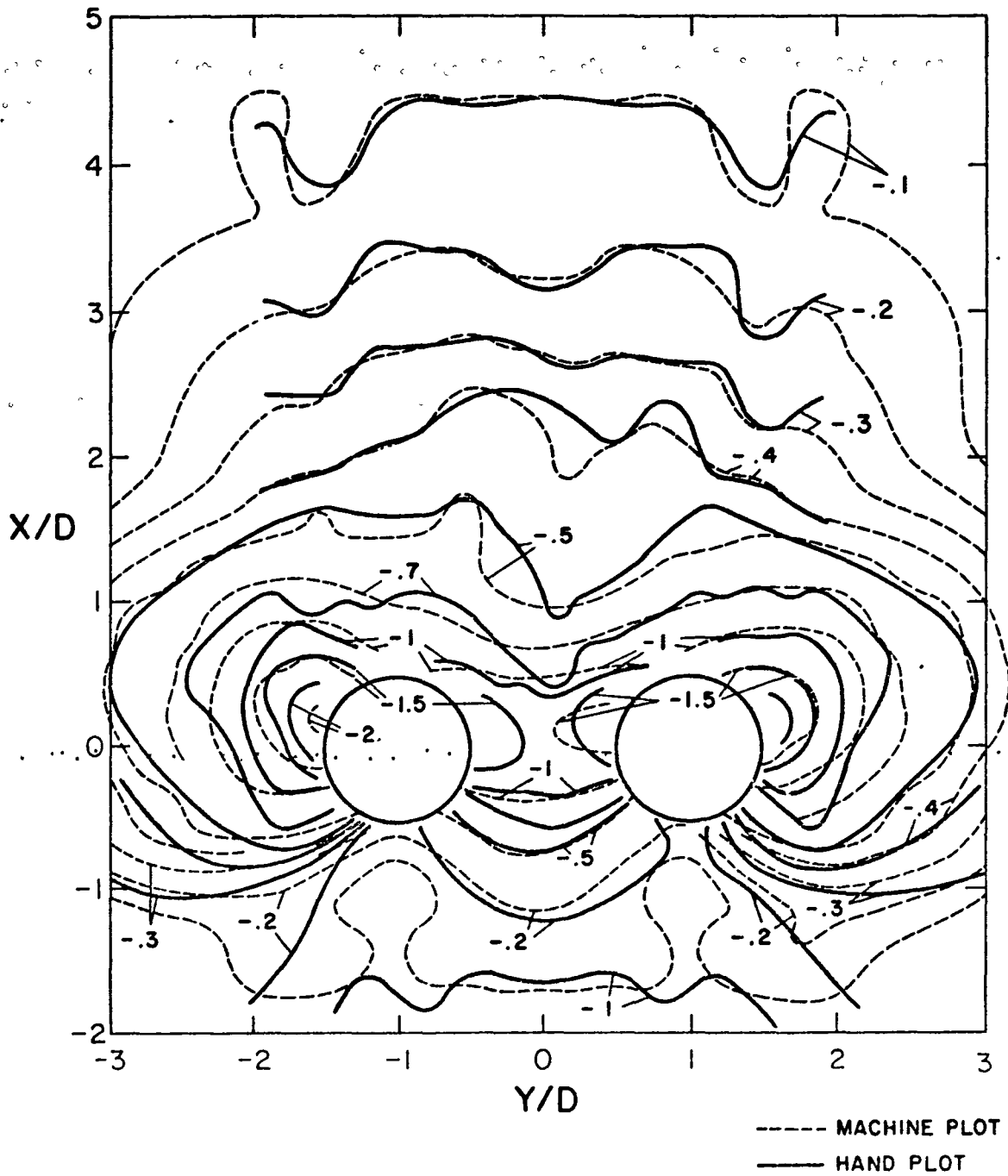


Fig. A1 Comparison of Computer- and Hand-Made Pressure Contours:
Side-by-Side Jets, Nonuniform Exit Profile, $\theta = 90^\circ$, $R = 4$

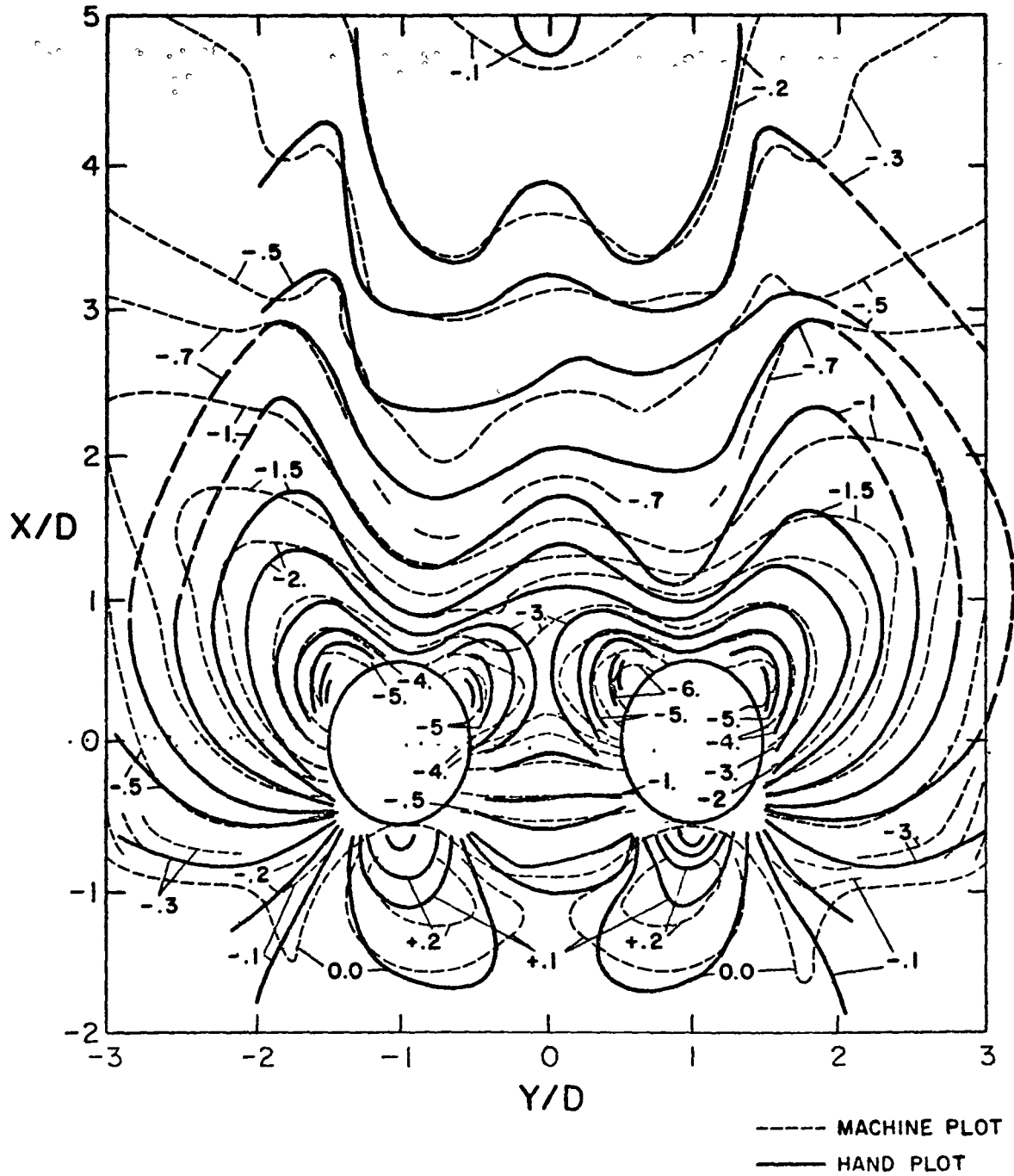


Fig. A2 Comparison of Computer- and Hand-Made Pressure Contours:
Side-by-Side Jets, Nonuniform Exit Profile, $\theta = 60^\circ$, $R = 4$

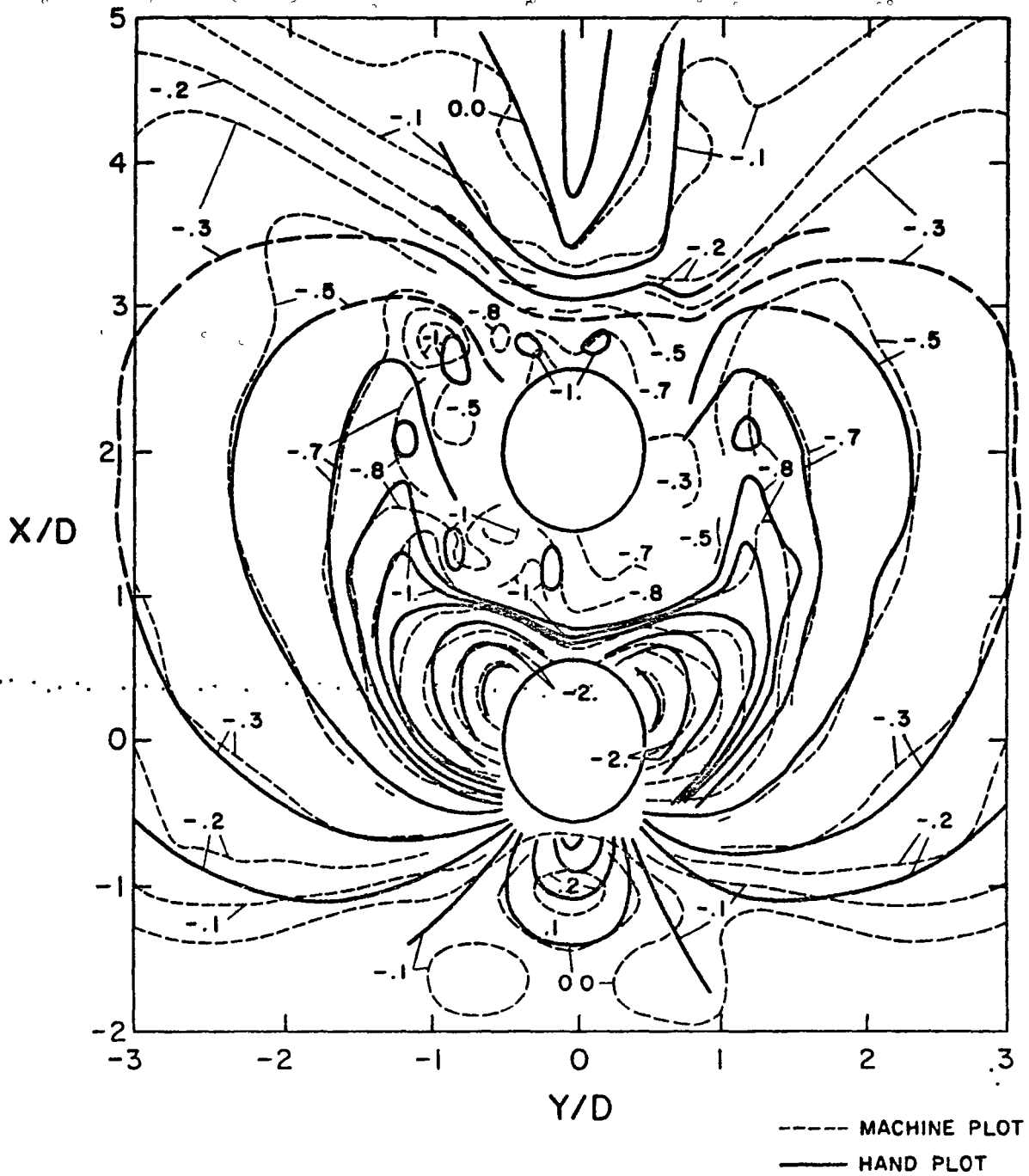


Fig. A3 Comparison of Computer- and Hand-Made Pressure Contours:
Tandem Jets, Nonuniform Exit Profile, $\theta = 60^\circ$, $R = 4$

END

DATE

FILMED

JAN 22 1986

End of Document